but the effect was not specific to CD11b$^+$ IgA$^+$ PCs (Fig. 3a). These data suggested that CD11b$^+$ IgA$^+$ PCs were not recent emigrants from IgA inductive tissues (for example, PPs and PerC).

The second possibility was that CD11b$^+$ IgA$^+$ PCs originated from B1 cells, because CD11b is a marker of peritoneal B1 cells[26]. To test this possibility, peritoneal CD11b$^+$ B1 cells were purified and adoptively transferred into severe combined immunodeficiency mice. As we reported previously[11], adoptively transferred CD11b$^+$ B1 cells migrated into the intestine, where they differentiated into IgA$^+$ PCs. Although we transferred B cells expressing CD11b, they lost their CD11b expression in the iLP (Supplementary Fig. S5). Although only a few cells were detected in the iLP under these experimental conditions, CD11b expression was likely to be reversible on B cells and was thus not to be a marker of PCs originating from peritoneal CD11b$^+$ B1 cells.

As a third possibility for discriminating between CD11b$^+$ and CD11b$^-$ IgA$^+$ PCs, we examined the T cell dependency of their differentiation and IgA production. For this, we employed TCRβδ mice. Although TCRβ δ mice had decreased levels of intestinal IgA$^+$ cells, the ratio between CD11b$^+$ and CD11b$^-$ IgA$^+$ PCs did not differ between the WT mice and the TCRβ δ mice (Fig. 3b).

We also examined the production of IgA against T cell dependent and T cell independent antigens by CD11b$^+$ and CD11b$^-$ IgA$^+$ PCs. For the analysis of T cell dependent antigen, mice were orally immunized with ovalbumin (OVA) plus cholera toxin (CT). Following three oral immunizations, substantial amounts of OVA-specific IgA antibody-forming cells (AFCs) were detected in the iLP by enzyme-linked immunosorbent spot (ELISPOT) assay; this production was reduced by almost 50% when either the CD11b$^+$ IgA$^+$ or the CD11b$^-$ IgA$^+$ cells were removed before the ELISPOT assay (Fig. 3c). Similar results were obtained when we enumerated IgA AFCs against phosphorylcholine, a typical TI antigen, induced by commensal bacteria (Fig. 3c)[27]. These results collectively suggested that both CD11b$^+$ IgA$^+$ and CD11b$^-$ IgA$^+$ cells almost equally included IgA AFCs producing IgA antibodies specific for T cell dependent and T cell independent antigens.

Next, to examine the involvement of PPs, we established PP-null mice by *in utero* treatment with anti-IL-7Rα antibody[28] and found that PP-null mice had reduced numbers of CD11b$^+$ IgA$^+$ PCs in the iLP (Fig. 3d). In addition, CD11b was not expressed on IgA$^+$ B cells in the PPs (Fig. 3e). We treated mice with anti-IL-7Rα antibody only once *in utero* and confirmed that it did not affect the ILFs[28]. Although it is still possible that CD11b$^+$ IgA$^+$ PCs specifically require IL-7, the most plausible conclusion based on our current findings is that CD11b$^+$ IgA$^+$ B cells require the lymphoid structure of PPs, and CD11b$^-$ IgA$^+$ B cells acquire CD11b expression in the iLP.

As in antibiotic-treated and MyD88 KO mice (Fig. 1), the numbers of CD11b$^-$ IgA$^+$ PCs changed little in PP-null mice (Fig. 3d), suggesting that it is unlikely that CD11b$^+$ IgA$^+$ PCs differentiate back into CD11b$^-$ IgA$^+$ cells in the iLP. This view is further supported by the results of *in vitro* analysis. When purified CD11b$^+$ and CD11b$^-$ IgA$^+$ PCs were separately cultured with different kinds of stimulants (for example, phorbol 12-myristate 13-acetate plus ionomycin, or lipopolysaccharide) little change was noted in CD11b expression (Supplementary Fig. S6). Although the origin of these cells remains to be firmly established, it is plausible that CD11b$^+$ IgA$^+$ PCs act as a separate lineage once they differentiate in the iLP.

High proliferation activity of CD11b$^+$ IgA$^+$ PCs. We next performed a gene microarray analysis to assess the uniqueness of CD11b$^+$ IgA$^+$ PCs in the iLP. Gene ontology enrich-

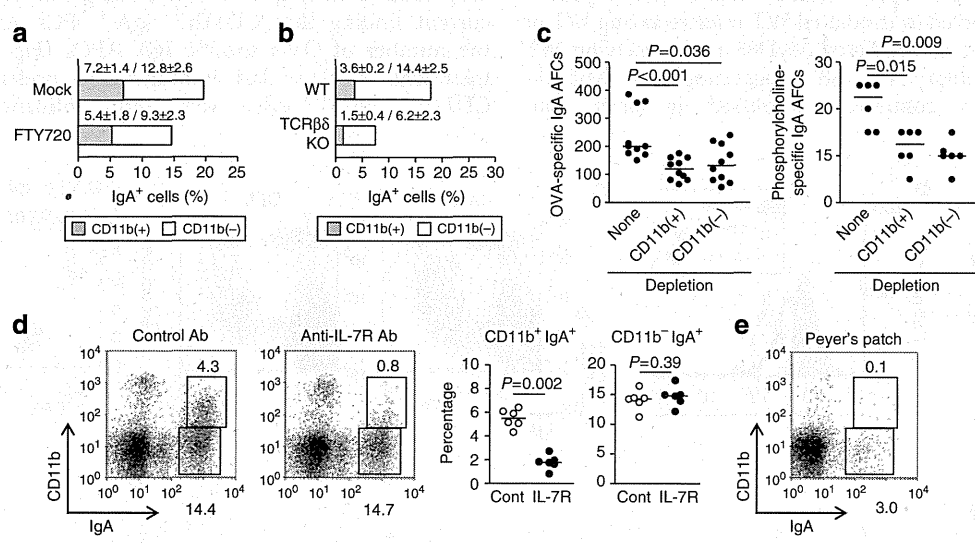

Figure 3 | CD11b$^+$ IgA$^+$ cells require the lymphoid structure of Peyer's patches. (**a**) Mice were treated with FTY720 every day for 5 days. The day after the final treatment, the proportions of CD11b$^+$ and CD11b$^-$ IgA$^+$ cells were measured by flow cytometry. Data are presented as means ± s.d. from four mice. Similar results were obtained from three separate experiments. (**b**) Proportions of CD11b$^+$ and CD11b$^-$ IgA$^+$ cells in the iLP of WT and TCRβδ KO mice were measured by flow cytometry. Data are presented as means ± s.d. from four mice. Similar results were obtained from three separate experiments. (**c**) After three oral immunizations with OVA plus cholera toxin, cells were isolated from the iLP and used in an ELISPOT assay to enumerate OVA-specific IgA AFCs. In some groups of mice, CD11b$^+$ or CD11b$^-$ IgA$^+$ cells were depleted by cell sorting before application of ELISPOT assay. Phosphorylcholine-specific IgA AFCs were measured. Graphs show data from individual mice, and bars indicate median. Statistical analyses were performed with Mann–Whitney's *U*-test. (**d**) Mononuclear cells were isolated from the iLP of Peyer's patch (PP)-normal (control Ab) and -null (anti-IL-7Rα Ab) mice for analysis of IgA and CD11b expression by flow cytometry. Graphs show data from individual mice. Statistical analyses were performed with Mann–Whitney's *U*-test. (**e**) Mononuclear cells were isolated from PPs for analysis of CD11b$^+$ and CD11b$^-$ IgA$^+$ cells by flow cytometry. Similar results were obtained from three separate experiments.

ment score computation analysis showed that the activity of cell-cycle-associated pathways was higher in CD11b$^+$ IgA$^+$ PCs than in CD11b$^-$ IgA$^+$ PCs (Supplementary Table S1). Consistent with this finding, higher expression of cell-cycle-associated genes was noted in CD11b$^+$ IgA$^+$ PCs than in CD11b$^-$ IgA$^+$ PCs; these genes included members of the cell division cycle family (Fig. 4a and Supplementary Table S2). In line with this, these cells expressed higher levels of the proliferation marker Ki67 than did CD11b$^-$ IgA$^+$ PCs (Fig. 4a and Supplementary Table S2). Additionally, CD11b$^+$ IgA$^+$ PCs showed greater uptake of bromodeoxyuridine (BrdU) than did CD11b$^-$ IgA$^+$ PCs (Fig. 4b). CD11b$^+$ IgA$^+$ PCs were preferentially removed by treatment with cyclophosphamide (CPM), which selectively targets proliferating cells (Fig. 4c). These data collectively suggested that CD11b$^+$ IgA$^+$ PCs possessed greater proliferating activity than did CD11b$^-$ IgA$^+$ PCs in the iLP.

Microarray analysis further identified CD150 (also known as signalling lymphocytic activation molecule family member 1, SLAMF1)[29], β1 integrin and CD168 (also known as hyaluronan-mediated motility receptor)[30] as possible candidates uniquely expressed on CD11b$^+$ IgA$^+$ PCs (Supplementary Table S3). Flow cytometric analysis confirmed that CD11b$^+$ IgA$^+$ PCs expressed higher levels of CD150 than did CD11b$^-$ IgA$^+$ PCs, whereas CD11b$^+$ IgA$^+$ and CD11b$^-$ IgA$^+$ PCs identically expressed β1 integrin and no CD168 (Supplementary Fig. S7).

IL-10 is essential for intestinal CD11b$^+$ IgA$^+$ cells. We next aimed to identify key molecules for inducing and maintaining CD11b$^+$ IgA$^+$ PCs in the iLP. As CD11b$^+$ IgA$^+$ PC numbers were reduced in MyD88 mice (Fig. 1c), and MyD88 is expressed in not only hematopoietic cells, including B cells, but also non-hematopoietic cells, including epithelial cells[31], we performed BM chimeric experiments to determine whether MyD88 in non-hematopoietic cells, hematopoietic cells, or both, was required for the generation of CD11b$^+$ IgA$^+$ cells. Similar levels of CD11b$^+$ IgA$^+$ cells were observed in irradiated WT mice receiving WT or MyD88 BM cells and in irradiated MyD88 mice receiving WT BM cells (Supplementary Fig. S8), suggesting that MyD88-dependent molecules commonly expressed in both non-hematopoietic and hematopoietic cells are involved in the microbe-dependent induction of CD11b$^+$ IgA$^+$ PCs.

We then examined the involvement of cytokines known to enhance IgA responses. Among several IgA-enhancing cytokines (for example, IL-5, IL-6, IL-10 and APRIL/BAFF)[7,15], we found that neutralization of IL-10 resulted in preferential reduction in CD11b$^+$ IgA$^+$ PCs, whereas blocking of other cytokines induced a reduction in IgA$^+$ cell numbers regardless of CD11b expression (Fig. 5a). Additionally, CD11b$^+$ IgA$^+$ cell numbers were preferentially reduced in IL-10 KO mice (Fig. 5b). As normal differentiation into IgA$^+$ B cells was observed in the PPs and PerC of IL-10 KO mice (Supplementary Fig. S9), it is plausible that IL-10 targets the maintenance of CD11b$^+$ IgA$^+$ cells in the iLP, but not the induction of IgA$^+$ cells in inductive tissues such as PPs and PerC.

Early-phase robust IgA responses by proliferating IgA$^+$ PCs. To examine the immunological importance of proliferating IgA$^+$ PCs present mainly in CD11b$^+$ IgA$^+$ PCs, mice were orally immunized with OVA plus CT. In this assay, one group received CPM treatment during immunization and the second group received CPM treatment 4 days after the final immunization (Fig. 6a). Because of the high cell-proliferation activity, CPM treatment during oral immunization resulted in efficient killing of peanut agglutinin (PNA^{hi}) B220$^+$ GC B cells and thus a reduction in the numbers of IgA$^+$ IgM$^-$ plasmablasts in the PPs (Supplementary Fig. S10). Thus, treatment with CPM during oral immunization led to an ~90% reduction in the numbers of OVA-specific IgA AFCs (Fig. 6b); this was associated with almost complete disappearance of faecal IgA produced against OVA (Fig. 6c). On the other hand, when mice were treated with CPM 4 days after the final immunization to remove proliferating cells mainly present in CD11b$^+$ IgA$^+$ cells in the iLP, the reduction in numbers of OVA-specific IgA AFCs in the iLP was only about 50% (Fig. 6b). This finding was consistent with our current finding that CD11b$^+$ IgA$^+$ PCs accounted for half the number of OVA-specific IgA AFCs (Fig. 3c). Thus, CPM treatment after the last immunization preferentially depleted CD11b$^+$ IgA$^+$ cells, with little influence on CD11b$^-$

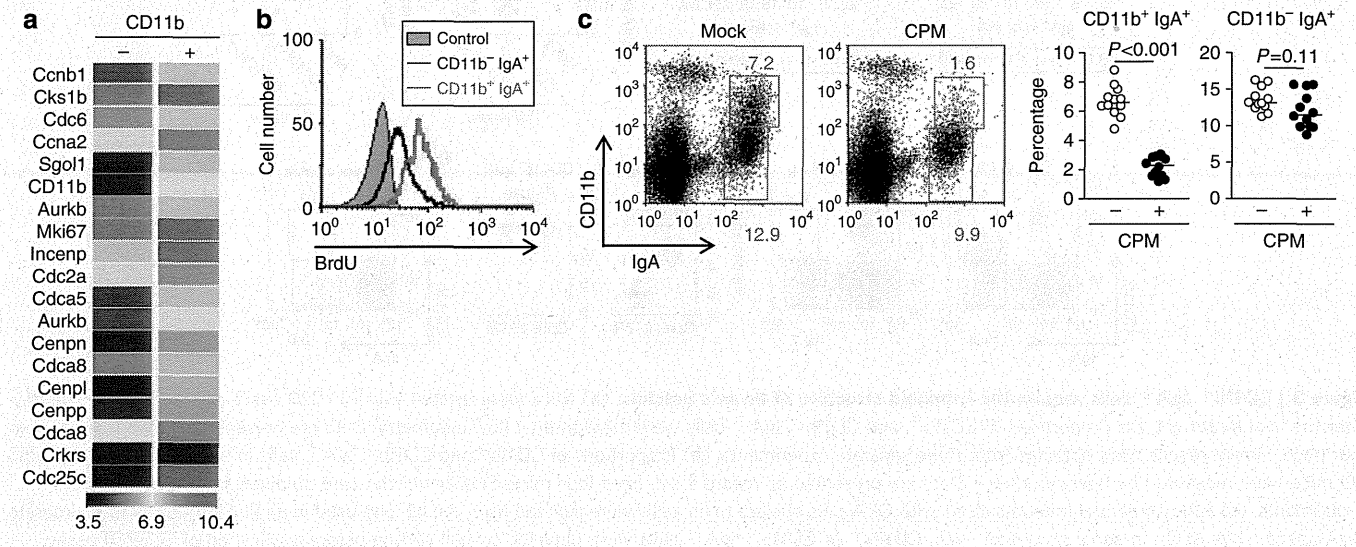

Figure 4 | CD11b$^+$ IgA$^+$ cells are proliferating cells. (**a**) mRNA was purified from small intestinal CD11b$^+$ and CD11b$^-$ IgA$^+$ cells and used for microarray analysis. Data related to the cell cycle and proliferation are shown. Data are representative of two independent experiments. (**b**) Mice were treated with BrdU, and uptake of BrdU by CD11b$^+$ and CD11b$^-$ IgA$^+$ cells was determined by flow cytometry. Data are representative of four independent experiments. (**c**) Cells were isolated from the intestinal lamina propria of mice receiving CPM to analyse CD11b$^+$ IgA$^+$ cells. Similar results were obtained from four separate experiments. Graphs show data from individual mice. Statistical analyses were performed with Mann-Whitney's *U*-test.

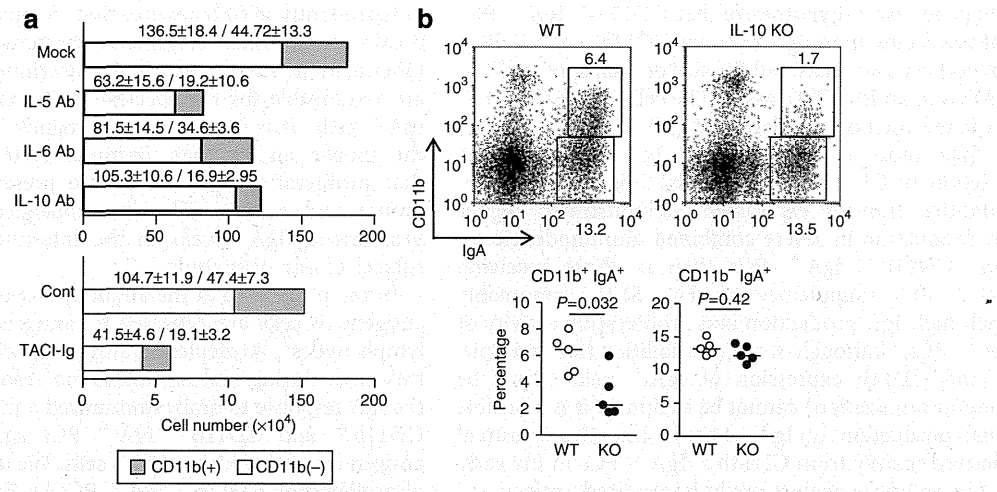

Figure 5 | Role of IL-10 in the maintenance of CD11b$^+$ IgA$^+$ cells in the iLP. (**a**) Mice were treated with antibodies to block IL-5, IL-6, IL-10 or antagonistic TACI-immunoglobulin (TACI-Ig) fusion protein. Mononuclear cells were isolated from the iLP and used for analysis of CD11b$^+$ and CD11b$^-$ IgA$^+$ cells by flow cytometry. Data are presented as means ± s.d. ($n=4$). (**b**) Mononuclear cells were isolated from the iLP of WT or IL-10 KO mice for analysis of IgA and CD11b expression by flow cytometry. Graphs show data from individual mice. Statistical analyses were performed with Mann–Whitney's *U*-test.

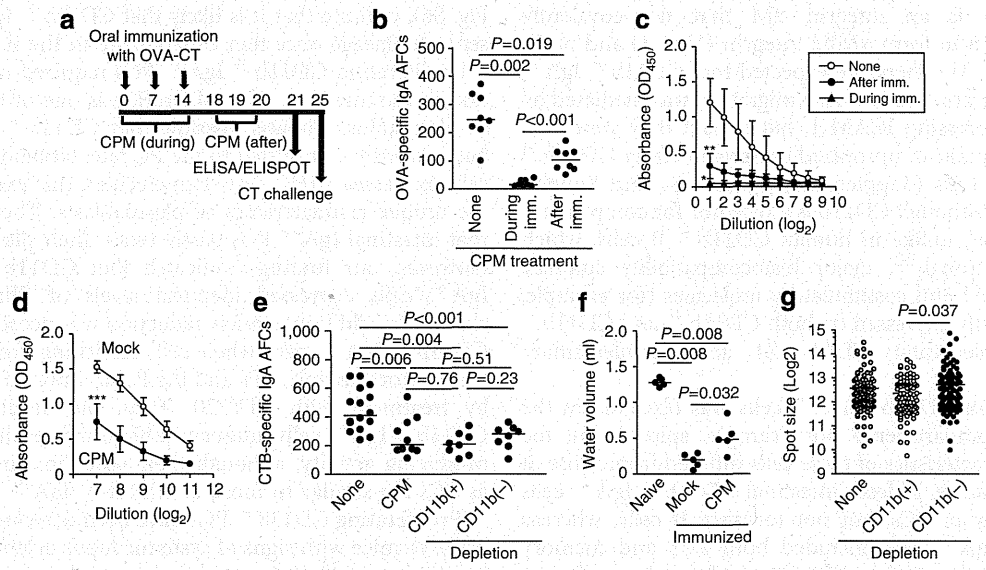

Figure 6 | Proliferating IgA$^+$ cells mediate early-phase IgA responses to oral antigen. (**a**) Experimental schedule for oral immunization and CPM treatment. Mice were orally immunized with OVA plus CT on days 0, 7 and 14. One group received CPM during oral immunization (days 0, 7 and 14) and another received CPM after the last immunization (days 18, 19 and 20). (**b**,**c**) One week after the final immunization (day 21), mononuclear cells were isolated from the iLP to quantify OVA-specific IgA-forming cells by ELISPOT (**b**). Simultaneously, faeces (**c**,**d**) were collected and were used for the detection of the (**c**) OVA-or (**d**) B subunit of CT (CTB)-specific IgA by enzyme-linked immunosorbent assay. Data are from individual mice and bars indicate median (**b**) and represent means ± s.d. ($n=10$) from two separate experiments (**c**,**d**). *$P<0.001$, **$P<0.01$, ***$P<0.05$ (two tailed unpaired *t*-test). (**e**) Mononuclear cells were isolated from the iLP of mock- or CPM-treated mice 1 week after the final immunization to quantify CTB-specific IgA-forming cells by ELISPOT. In some groups of mock-treated mice, CD11b$^+$ or CD11b$^-$ IgA$^+$ cells were depleted by cell sorting before application of ELISPOT assay. Graphs show data from individual mice, and bars indicate median. (**f**) On day 21, mice were orally challenged with 100 μg CT. After 15 h, the volume of intestinal fluid was measured. Graphs show data from individual mice, and bars indicate median. Similar results were obtained from two separate experiments. (**g**) Spot sizes of CTB-specific IgA AFCs were measured by Zeiss KS ELISPOT software. Graphs show data from individual mice, and bars indicate median. Statistical analyses were performed with Mann–Whitney's *U*-test (**e**–**g**).

IgA$^+$ cells. Of note, these mice showed ~90% reduction in OVA-specific IgA content in the faeces compared with mice not treated with CPM (Fig. 6c). We also confirmed that CPM treatment 4 days after final immunization induced a reduction in the production of IgA specific to the B subunit of CT (that is, CTB), which was associated with the halving of the abundance of CTB-specific IgA AFCs in the intestine (Fig. 6d,e). Like OVA-specific IgA responses (Figs. 3c and 6b), similar levels of reduction of CTB-specific IgA AFCs were noted when CD11b$^+$ IgA$^+$ cells were depleted before ELISPOT assay (Fig. 6e). These mice showed reduced resistance to oral challenge with CT and developed watery diarrhoea (Fig. 6f and Supplementary Fig. S11).

These findings led us to hypothesize that CD11b$^+$ IgA$^+$ PCs are capable of producing more IgA than are CD11b$^-$ IgA$^+$ PCs. To test this hypothesis, we measured the size of each spot in CTB-specific IgA AFCs in an ELISPOT assay. The cells in the CD11b$^+$ IgA$^+$ cell-enriched fraction (depletion of CD11b$^-$ IgA$^+$ cells) were bigger than those in the CD11b$^-$ IgA$^+$ cell-enriched fraction (depletion of CD11b$^+$ IgA$^+$ cells) (Fig. 6g). Furthermore, an adoptive transfer experiment demonstrated higher intestinal IgA production in severe combined immunodeficiency mice receiving CD11b$^+$ IgA$^+$ PCs than in those receiving CD11b$^-$ IgA$^+$ PCs (Supplementary Fig. S12), presumably because of both high IgA production and proliferating activity of CD11b$^+$ IgA$^+$ PCs. Although some possibilities (for example, proliferation and CD11b expression of IgA$^+$ cells might be changed during immunization) cannot be excluded, it is plausible that the actual production of IgA secreted into the intestinal lumen was derived mainly from CD11b$^+$ IgA$^+$ PCs in the early phase of the IgA response against orally immunized antigen.

Discussion

PCs could secrete antibodies to provide antigen-specific humoral immune responses in both systemic and mucosal tissues. Here, we demonstrated that intestinal IgA$^+$ PCs in mice could be categorized into two populations on the basis of CD11b expression. CD11b is an integrin αM that non-covalently associates with CD18 to form αMβ2 integrin (Mac-1) and binds to ICAM-1 (ref. 24). We therefore expected that CD11b$^+$ IgA$^+$ PCs were newly migrating cells whose migration was mediated by endothelial cells expressing ICAM-1, but in fact they were not. We also found no uptake of opsonized bacteria in either CD11b$^+$ or CD11b$^-$ IgA$^+$ cells (Supplementary Table S4 and Supplementary Fig. S13a), although CD11b is a receptor for complement (iC3b)[24]. In addition, unlike in human CD11b$^+$ B cells, which stimulate T cells strongly[32], major histocompatibility complex (MHC) class II (I-A^d) and costimulatory molecules (for example, CD80) were identically expressed on both CD11b$^+$ and CD11b$^-$ IgA$^+$ cells (Supplementary Table S4 and Supplementary Fig. S13b).

A similar subset of CD11b$^+$ IgA$^+$ cells was observed in the systemic murine compartments (for example, spleen), but the immunological characteristics of these cells differed from those of the cells in the intestine. Indeed, intestinal CD11b$^+$ IgA$^+$ cells consisted exclusively of PCs, but not memory B cells, whereas splenic CD11b$^+$ IgA$^+$ cells included both PCs and memory B cells. We further found that CD11b could not be used as a marker of B1 cells in the intestine. Our current findings show for the first time that CD11b could be a specific marker for discriminating IgA$^+$ PCs that require microbial stimulation and IL-10, and presumably contribute to the early phase of the intestinal IgA response in mice.

We have identified unique CD11b$^+$ IgA$^+$ PCs in mice; the next question is whether or not the same population of IgA$^+$ PCs exists in humans. Our preliminary experiments have shown that no human intestinal IgA$^+$ cells express CD11b, but that some IgA$^+$ cells express Ki67, a marker of proliferating cells (unpublished data). One possible explanation for this difference between human and mice is difference in the composition of commensal bacteria. In this regard, we examined the involvement of segmented filamentous bacteria (SFB), which are a known major IgA stimulus in mice, but has not yet been confirmed as part of the human microbiota[19]. As expected, SFB stimulated IgA production following colonization of SFB-deficient C57BL/6 mice from the Jackson laboratory (JAX mice) with bacterial suspensions from SFB-monoassociated mice (JAX + SFB mice)[33]; however, we found that CD11b is expressed on IgA$^+$ cells independently of SFB colonization (Supplementary Fig. S14). It is possible that other commensal bacteria such as *Lactobacillus* (abundant in mice) and *Bifidobacterium* (abundant in human) are responsible for the species-specific expression of CD11b on IgA$^+$ cells. It is important to recognize the differences between the mouse and human immune systems, but it is obvious that proliferating IgA$^+$ cells are present in the iLP of both mouse and human. The immunological function of human proliferating IgA$^+$ cells in the intestine will therefore be the subject of our next study.

In the initial step of the antibody response to T cell dependent antigens, B cells are activated by antigens and form GCs in the lymph nodes[7]. As depleting antigen-specific GC B cells by CPM treatment during oral immunization resulted in complete loss of the IgA response to orally immunized antigen, it is likely that both CD11b$^+$ and CD11b$^-$ IgA$^+$ PCs against T cell dependent antigen are derived from GC B cells. We also found that depletion of proliferating CD11b$^+$ IgA$^+$ PCs by CPM treatment after final immunization led to a decrease in the early-phase IgA response, although it is possible that proliferation activity and/or CD11b expression on IgA$^+$ cells might be wobble during immunization. Our *in vivo* findings indicated that the reduction in CD11b$^+$ IgA$^+$ PC numbers in MyD88 KO, IL-10 KO and PP-null mice did not affect the numbers of CD11b$^-$ IgA$^+$ PCs (Figs 1c, 3d and 5b). These findings, together with our *in vitro* data (Supplementary Fig. S6), indicate that it is likely that CD11b$^+$ IgA$^+$ PCs act as a separate lineage once they differentiate in the iLP.

Proliferating CD11b$^+$ IgA$^+$ PCs required microbial stimulation in the intestine. As proliferation is one of the characteristics of plasmablasts, it was possible that CD11b$^+$ IgA$^+$ cells have been recently committed to the PC fate. Notably, intestinal IgA$^+$ cells expressed MHC class II molecules; this expression is one of the unique characteristics of plasmablasts. Therefore, it is likely that intestinal IgA$^+$ PCs partly retain their plasmablast features. However, our findings indicated that CD11b$^+$ and CD11b$^-$ IgA$^+$ cells expressed identical levels of Blimp-1 and MHC class II. In addition, similar reduction was noted in CD11b$^+$ and CD11b$^-$ IgA$^+$ cells when cell trafficking from IgA inductive tissues (for example, PPs and the PerC) into the iLP was inhibited by treatment with FTY720. Thus, our findings suggest that CD11b$^+$ IgA$^+$ cells uniquely exhibit high proliferating and IgA-producing activity, although their other immunological features as PCs are similar to those of CD11b$^-$ IgA$^+$ PCs.

Proliferating CD138$^+$ PCs have been detected in the spleens of NZB/W mice with signs of systemic lupus erythematosus, but not in naive mice[34]. In contrast, the number of non-proliferating CD138$^+$ PCs is unchanged in the intestines of GF mice, as it is in the spleens of NZB/W mice[34]. These findings suggest that MyD88-dependent homeostatic stimulation of commensal bacteria determines the fate of proliferating CD11b$^+$ IgA$^+$ CD138$^+$ PCs in the intestine. Several lines of evidence have revealed the cellular and molecular mechanisms of microbe-dependent initiation of IgA responses. B cells express several toll-like receptors, and B cell-intrinsic MyD88-mediated signalling has been implicated in enhanced antibody production in some studies[35,36]. However, our current findings indicated that MyD88-mediated signalling in hematopoietic cells, including B cells, was not essential for intestinal CD11b$^+$ IgA$^+$ PC production. Additionally, we found IL-10 as a key molecule inducing CD11b$^+$ IgA$^+$ PC production. Previous studies have demonstrated that IL-10 promotes the proliferation of activated B cells and subsequent IgA production *in vitro*[37,38], which are consistent with our current findings of high-level proliferation of, and IgA production by, CD11b$^+$ IgA$^+$ PCs. Thus, our current findings proved that IL-10 functions in IgA production *in vivo* and that CD11b$^+$ IgA$^+$ PCs are the main targets in this

pathway. Despite these findings, our preliminary study demonstrated that treatment of CD11b$^+$ or CD11b$^-$ IgA$^+$ PCs with IL-10 alone did not induce their reciprocal differentiation into each other, and IL-10 KO mice with colitis possessed CD11b$^+$ IgA$^+$ PCs (J.K., unpublished data). Thus, IL-10 is redundant in some cases and additional factors are required for the maintenance of CD11b$^+$ IgA$^+$ PCs. Our current findings identified CD150 as a surface molecule that is highly expressed on CD11b$^+$ IgA$^+$ PCs. CD150 is a 70-kDa glycoprotein expressed on some B and T cells, thymocytes and macrophages[29]. Homophilic interaction of CD150 induces proliferation of, and antibody synthesis by, B cells[39], and notably IL-10 synergistically enhances CD150-mediated B cell proliferation[39]. Thus, it is likely that, at least partly, IL-10 and CD150 determine the unique features (for example, proliferation and high IgA production) of CD11b$^+$ IgA$^+$ PCs in the iLP. In addition, accumulating evidence has revealed an important immunological function of stromal cells as survival niches for PCs in the BM[40] and intestine[41,42]. It is possible that complex immunological communications among commensal flora, epithelial and stromal cells, and the cells involved in innate and acquired immunity determine the differentiation and maintenance of IgA PCs in the intestine.

Taken together, our results provide new insights into the nature of IgA$^+$ PCs in the murine intestine, and especially into the regulation of the early-phase IgA responses to intestinal antigens and requirement of microbe-dependent stimulation, IL-10, and the PP lymphoid structure. These findings add a new level of complexity to the intestinal IgA system of mice.

Methods

Mice. SPF and GF Balb/c mice were obtained from Japan CLEA (Tokyo, Japan). MyD88 KO mice, IL-10 mice (Balb/c background) and TCRβδ mice (C57/BL6 background) were maintained under SPF conditions at the Experimental Animal Facility, The Institute of Medical Science, The University of Tokyo, and WT littermates were used as controls. To deplete gut commensal bacteria, mice received broad-spectrum antibiotics, namely ampicillin (1 g l^{-1}; Sigma-Aldrich, St Louis, MO), vancomycin (500 mg l^{-1}; Shionogi, Osaka, Japan), neomycin sulphate (1 g l^{-1}; Sigma-Aldrich) and metronidazole (1 g l^{-1}; Sigma-Aldrich), in their drinking water for 4 weeks[43]. To establish BM chimeric mice, we injected γ-irradiated (960 rad, Gammacell 40, Atomic Energy of Canada Limited, Ontario, Canada) recipient mice with 5×10^6 BM cells through the tail vein and used them in experiments 8 weeks after injection. Under our experimental conditions, the reconstitution efficacy was about 90–95%. To obtain PP-null mice, pregnant BALB/c mice were injected intravenously and subcutaneously with 1 mg anti-IL-7Rα antibody (A7R34, BioLegend, San Diego, CA) at 14.5 days post coitus, as described previously[28]. We confirmed the disruption of organized PPs and the existence of ILFs in the offspring, as described previously[28]. To neutralize cytokines, mice were treated intraperitoneally with 250 μg of monoclonal antibodies specific for IL-5 (TRFK5), IL-6 receptor (D7715A7) or IL-10 (JES5.16E3) (BioLegend, San Diego, CA); control antibody (Rat IgG2b); or 100 μg of soluble TACI-Fc fusion protein (R&D Systems, Minneapolis, MN) every second day for 2 weeks[44,45]. For assessing the role of SFB, mice purchased from the Jackson laboratory were orally inoculated with bacterial suspensions obtained by homogenizing faecal pellets from SFB-monoassociated mice in water. SFB colonization was confirmed by quantitative PCR[33] and CD11b$^+$ IgA$^+$ cells were analysed in the small intestine 2 weeks post gavage by flow cytometry. All experiments followed the guidelines of the Animal Care and Use Committee, The University of Tokyo and Columbia University.

Oral immunization. Mice were given sodium bicarbonate solution to neutralize stomach acid[11,13]. Thirty minutes later, the mice were orally immunized with 1 mg OVA (Sigma-Aldrich) and 10 μg CT (List Biological Laboratories, Campbell, CA). This procedure was conducted on days 0, 7 and 14. In some groups, mice were intraperitoneally given CPM (35 mg kg^{-1} each time, Sigma-Aldrich). One week after the final immunization, faecal samples and mononuclear cells from the iLP were collected for enumeration of OVA-specific antibody responses by enzyme-linked immunosorbent assay and ELISPOT, respectively[13]. *In vivo* CT challenge was performed by oral challenge of naive or immunized mice with 100 μg of CT as previously described[46].

Cell isolation. To isolate mononuclear cells from PPs, we stirred the tissues in RPMI-1640 medium containing 2% fetal calf serum plus 0.5 mg ml^{-1} collagenase (Wako, Osaka, Japan)[11,13]. To isolate mononuclear cells from the iLP, PPs were carefully removed and the remaining intestines including ILFs were opened longitudinally, washed with RPMI-1640, cut into 2-cm pieces and stirred for 20 min at 37 °C into RPMI-1640 containing 0.5 mM EDTA and 2% fetal calf serum to remove epithelial cells and intraepithelial lymphocytes[11,13]. The tissues were then stirred three times in 0.5 mg ml^{-1} collagenase for 20 min before undergoing discontinuous Percoll gradient centrifugation (40 and 75%). Peritoneal cells were obtained by peritoneal flushing with 8 ml ice-cold phosphate-buffered saline (PBS)[11,13].

Flow cytometry and cell sorting. Mononuclear cells were preincubated with 10 μg ml^{-1} anti-CD16/32 antibody (BD Biosciences, San Diego, CA). They were then reacted with the following antibodies: Pacific blue-rat anti-mouse CD45R (B220) (RA3-6B2, 0.8 μg ml^{-1}), phycoerythrin (PE)-rat anti-mouse CD11b (M1/70, 0.1 μg ml^{-1}), PE-Cy7-hamster anti-mouse CD11c (HL3, 0.4 μg ml^{-1}), PE-rat anti-mouse CD18 (C71/16, 0.8 μg ml^{-1}), PE-rat anti-mouse CD19 (1D3, 0.8 μg ml^{-1}), PE-rat anti-mouse CD38 (90, 0.13 μg ml^{-1}), FITC-rat anti-mouse IgA (C10-3, 2 μg ml^{-1}), PE-Cy7-rat anti-mouse IgM (R6-60.2, 1 μg ml^{-1}), PE-anti-mouse I-A^d (AMS-32.1, 0.4 μg ml^{-1}), APC-Cy7-rat anti-mouse CD11b (M1/70, 1 μg ml^{-1}), APC-Cy7-anti-mouse β1-integrin (HMβ1-1, 4 μg ml^{-1}), APC-anti-mouse CD40 (3/23, 2 μg ml^{-1}), Pacific blue-anti-mouse CD11b (M1/70, 1 μg ml^{-1}), PE-Cy7-anti-mouse F4/80 (BM8, 0.4 μg ml^{-1}) and biotin mouse anti-CD138 (281-2, 10 μg ml^{-1}) (all antibodies from BD Biosciences) followed by incubation with streptavidin-APC (1 μg ml^{-1}, BD Biosciences), PE-anti-mouse CD150 (TC15-12F12.2, 0.1 μg ml^{-1}), Alexa Fluor 647-anti-mouse CD80 (16-10A1, 1 μg ml^{-1}) (BioLegend, San Diego, CA), anti-mouse CD267 (TACI) (8F10-3, 4 μg ml^{-1}) (eBioscience, San Diego, CA), PE-mouse CCR3 (83101, 0.5 μg ml^{-1}) (R&D Systems) or biotinylated anti-peanut agglutinin lectin (1 μg ml^{-1}, Vector Laboratories, Burlingame, CA), followed by staining with streptavidin PE (1 μg ml^{-1}, BD Biosciences). For staining for Blimp-1, cells were fixed and permeabilized with a Cytofix/Cytoperm kit (BD Biosciences) and stained with PE-conjugated anti-Blimp1 goat polyclonal IgG (0.4 μg ml^{-1}, Santa Cruz Biotechnology, Santa Cruz, CA). FSC-H and FSC-A discrimination was used to exclude doublet cells, and ViaProbe cell-viability solution (BD Biosciences) was used to discriminate between dead and living cells. To detect proliferating cells, mice received 1 mg BrdU intraperitoneally 24 h before analysis; the BrdU signal was detected with the manufacturer's protocol (BD Biosciences). Concentration-matched isotype antibodies were used as negative controls. Flow-cytometric analysis and cell sorting were performed with FACSCanto II and FACSAria (BD Biosciences), respectively. We confirmed that cell purity was about 95% (Fig. 2a).

Immunohistological analysis. Intestines were fixed in 4% paraformaldehyde for 15 h at 4 °C, washed with PBS and treated sequentially in 10 and 20% sucrose for 12 h at 4 °C[13]. The tissues were embedded in OCT compound (Sakura Fine-technical Co., Tokyo, Japan). Cryostat sections (7 μm) were pre-blocked with anti-CD16 and CD32 antibody for 15 min at room temperature and stained for 15 h at 4 °C with FITC-rat anti-mouse IgA (C10-3, 2 μg ml^{-1}) and biotin anti-mouse CD11b antibody (M1/70, 1 μg ml^{-1}). This was followed by incubation with horseradish peroxidase (HRP)-conjugated streptavidin (Pierce, Rockford, IL) for 30 min at 4 °C and amplification of the fluorescent signal with Cy3-tyramide (TSA-Direct kit; PerkinElmer, Waltham, MA)[13]. We confirmed that no signal was detected when the specimens were stained with the concentration-matched isotype antibodies. They were then counterstained with 4′,6-diamidino-2-phenylindole (Sigma-Aldrich). Deconvoluted fluorescence images of specimens were obtained by fluorescence microscopy (BZ9000, Keyence, Osaka, Japan).

Detection of antibody responses by enzyme-linked immunosorbent assay and ELISPOT. To measure OVA- or CTB-specific IgA levels in faecal extracts, faeces were homogenized in PBS by vigorous vortexing[11,13]. After centrifugation of the extracts (9,000*g* for 15 min) the supernatants were used as faecal extracts. Plates were coated with 1 mg ml^{-1} OVA or 2 μg ml^{-1} CTB in PBS; this was followed by blocking for 1 h at room temperature with 200 μl PBS containing 1% (w/v) bovine serum albumin. After extensive washing of the plates with PBS containing 0.05% Tween 20, serial sample dilutions were added for incubation overnight at 4 °C. Samples were then incubated for 1 h at room temperature with optimally diluted HRP-conjugated goat anti-mouse IgA (SouthernBiotech, Birmingham, AL). After sample washing, the colour reaction was developed at room temperature with 3,3′,5,5′-tetramethylbenzidine (Moss, Pasadena, MD) and terminated by adding 0.5 M HCl. The colour reaction was measured as the optical density (wavelength 450 nm).

ELISPOT assay was used to enumerate IgA-producing AFCs in the iLP[11,13]. Briefly, various concentrations of mononuclear cells were cultured at 37 °C for 4 h in 96-well nitrocellulose membrane plates (Millititer HA; Millipore, Bedford, MA) coated with 1 mg ml^{-1} OVA and 5 μg ml^{-1} bovine serum albumin-conjugated phosphorylcholine (Biosearch Technologies, Novato, CA). After vigorous washing of the plates with PBS and PBS containing 0.05% Tween 20, HRP-conjugated goat anti-mouse IgA was added; the plates were then incubated overnight at 4 °C. Spots of AFCs were developed with 2-amino-9-ethylcarbazole

(Polysciences, Warrington, PA). The size of each spot was measured with Zeiss KS ELISPOT software (Oberkochen, Germany).

***In vitro* culture**. $CD11b^+$ IgA^+ or $CD11b^-IgA^+$ PCs (10^4 cells per well) were purified from the iLP and cultured with 100 ng ml^{-1} phorbol 12-myristate 13-acetate plus 300 ng ml^{-1} ionomycin, or 10 μg ml^{-1} lipopolysaccharide (all from Sigma-Aldrich), for 24 h.

For the bacteria uptake assay, fluorescent *Staphylococcus aureus* was opsonized in accordance with the manufacturer's protocol (Molecular Probes). Mononuclear cells isolated from the iLP (2×10^5 cells) were incubated with 1×10^5 opsonized bacteria for 90 min. After being washed, the cells were stained with antibodies for PE-IgA (mA-6E1, 0.5 μg ml^{-1}, eBioscience) and Pacific Blue CD11b, and the bacterial uptake by each population was examined by flow cytometry.

Microarray analysis. Microarray analysis was performed as we previously reported[47]. Briefly, $CD11b^+$ IgA^+ and $CD11b^-$ IgA^+ cells were isolated from the iLP, and total RNA was extracted from them with an RNeasy kit (Qiagen, Dusseldorf, Germany). cRNA was hybridized with DNA probes on a GeneChip Mouse Genome 430 2.0 array (Affymetrix), washed and fluorescence-labelled in accordance with the standard amplification protocol developed by Affymetrix. The fluorescence intensity of each probe was taken to represent the raw expression level and was quantified with GeneChip Operating software (Affymetrix). Data obtained from two independent experiments were analysed with GeneSpring 7.3.1 software (Silicon Genetics). All microarray data have been deposited in the National Center for Biotechnology Information Gene Expression Omnibus database (www.ncbi.nlm.nih.gov/geo/) under the accession no. GSE37225.

Statistics. Results were compared by a non-parametric Mann–Whitney's *U*-test and unpaired *t*-test (two tailed) (GraphPad Software, San Diego, CA).

References

1. Macpherson, A. J., McCoy, K. D., Johansen, F. E. & Brandtzaeg, P. The immune geography of IgA induction and function. *Mucosal Immunol.* **1,** 11–22 (2008).
2. Brandtzaeg, P. Function of mucosa-associated lymphoid tissue in antibody formation. *Immunol. Invest.* **39,** 303–355 (2010).
3. Fagarasan, S. Intestinal IgA synthesis: a primitive form of adaptive immunity that regulates microbial communities in the gut. *Curr. Top Microbiol. Immunol.* **308,** 137–153 (2006).
4. Macpherson, A. J. & Slack, E. The functional interactions of commensal bacteria with intestinal secretory IgA. *Curr. Opin. Gastroenterol.* **23,** 673–678 (2007).
5. Slack, E. *et al.* Innate and adaptive immunity cooperate flexibly to maintain host-microbiota mutualism. *Science* **325,** 617–620 (2009).
6. Woof, J. M. & Kerr, M. A. The function of immunoglobulin A in immunity. *J. Pathol.* **208,** 270–282 (2006).
7. Fagarasan, S., Kawamoto, S., Kanagawa, O. & Suzuki, K. Adaptive immune regulation in the gut: T cell-dependent and T cell-independent IgA synthesis. *Annu. Rev. Immunol.* **28,** 243–273 (2010).
8. Hayakawa, K., Hardy, R. R. & Herzenberg, L. A. Progenitors for Ly-1 B cells are distinct from progenitors for other B cells. *J. Exp. Med.* **161,** 1554–1568 (1985).
9. Kantor, A. B. & Herzenberg, L. A. Origin of murine B cell lineages. *Annu. Rev. Immunol.* **11,** 501–538 (1993).
10. Montecino-Rodriguez, E., Leathers, H. & Dorshkind, K. Identification of a B-1 B cell-specified progenitor. *Nat. Immunol.* **7,** 293–301 (2006).
11. Kunisawa, J. *et al.* Sphingosine 1-phosphate regulates peritoneal B-cell trafficking for subsequent intestinal IgA production. *Blood* **109,** 3749–3756 (2007).
12. Tsuji, M. *et al.* Requirement for lymphoid tissue-inducer cells in isolated follicle formation and T cell-independent immunoglobulin A generation in the gut. *Immunity* **29,** 261–271 (2008).
13. Gohda, M. *et al.* Sphingosine 1-phosphate regulates the egress of IgA plasmablasts from Peyer's patches for intestinal IgA responses. *J. Immunol.* **180,** 5335–5343 (2008).
14. Mora, J. R. *et al.* Generation of gut-homing IgA-secreting B cells by intestinal dendritic cells. *Science* **314,** 1157–1160 (2006).
15. Cerutti, A., Chen, K. & Chorny, A. Immunoglobulin responses at the mucosal interface. *Annu. Rev. Immunol.* **29,** 273–293 (2011).
16. Radbruch, A. *et al.* Competence and competition: the challenge of becoming a long-lived plasma cell. *Nat. Rev. Immunol.* **6,** 741–750 (2006).
17. Weinstein, P. D. & Cebra, J. J. The preference for switching to IgA expression by Peyer's patch germinal center B cells is likely due to the intrinsic influence of their microenvironment. *J. Immunol.* **147,** 4126–4135 (1991).
18. Hamada, H. *et al.* Identification of multiple isolated lymphoid follicles on the antimesenteric wall of the mouse small intestine. *J. Immunol.* **168,** 57–64 (2002).
19. Talham, G. L., Jiang, H. Q., Bos, N. A. & Cebra, J. J. Segmented filamentous bacteria are potent stimuli of a physiologically normal state of the murine gut mucosal immune system. *Infect. Immun.* **67,** 1992–2000 (1999).
20. Cebra, J. J., Jiang, H. Q., Boiko, N. V. & Tlaskalva-Hogenova, H. The role of mucosal microbiota in the development, maintenance, and pathologies of the mucosal immune system. in *Mucosal Immunology* 3rd edn (Mestecky, J. *et al.* eds) 335–368 (Academic Press, 2005).
21. Tezuka, H. *et al.* Regulation of IgA production by naturally occurring TNF/iNOS-producing dendritic cells. *Nature* **448,** 929–933 (2007).
22. Suzuki, K. *et al.* The sensing of environmental stimuli by follicular dendritic cells promotes immunoglobulin A generation in the gut. *Immunity* **33,** 71–83 (2010).
23. Shapiro-Shelef, M. & Calame, K. Regulation of plasma-cell development. *Nat. Rev. Immunol.* **5,** 230–242 (2005).
24. Patarroyo, M. *et al.* Leukocyte-cell adhesion: a molecular process fundamental in leukocyte physiology. *Immunol. Rev.* **114,** 67–108 (1990).
25. Pabst, O. *et al.* Cutting edge: egress of newly generated plasma cells from peripheral lymph nodes depends on beta 2 integrin. *J. Immunol.* **174,** 7492–7495 (2005).
26. Kunisawa, J. & Kiyono, H. A marvel of mucosal T cells and secretory antibodies for the creation of first lines of defense. *Cell Mol. Life Sci.* **62,** 1308–1321 (2005).
27. Shroff, K. E., Meslin, K. & Cebra, J. J. Commensal enteric bacteria engender a self-limiting humoral mucosal immune response while permanently colonizing the gut. *Infect. Immun.* **63,** 3904–3913 (1995).
28. Kunisawa, J. *et al.* Lack of antigen-specific immune responses in anti-IL-7 receptor alpha chain antibody-treated Peyer's patch-null mice following intestinal immunization with microencapsulated antigen. *Eur. J. Immunol.* **32,** 2347–2355 (2002).
29. Schwartzberg, P. L., Mueller, K. L., Qi, H. & Cannons, J. L. SLAM receptors and SAP influence lymphocyte interactions, development and function. *Nat. Rev. Immunol.* **9,** 39–46 (2009).
30. Maxwell, C. A., McCarthy, J. & Turley, E. Cell-surface and mitotic-spindle RHAMM: moonlighting or dual oncogenic functions? *J. Cell Sci.* **121,** 925–932 (2008).
31. Cario, E. *et al.* Lipopolysaccharide activates distinct signaling pathways in intestinal epithelial cell lines expressing Toll-like receptors. *J. Immunol.* **164,** 966–972 (2000).
32. Griffin, D. O. & Rothstein, T. L. A small CD11b(+) human B1 cell subpopulation stimulates T cells and is expanded in lupus. *J. Exp. Med.* **208,** 2591–2598 (2011).
33. Ivanov, I. I. *et al.* Induction of intestinal Th17 cells by segmented filamentous bacteria. *Cell* **139,** 485–498 (2009).
34. Hoyer, B. F. *et al.* Short-lived plasmablasts and long-lived plasma cells contribute to chronic humoral autoimmunity in NZB/W mice. *J. Exp. Med.* **199,** 1577–1584 (2004).
35. Pasare, C. & Medzhitov, R. Control of B-cell responses by Toll-like receptors. *Nature* **438,** 364–368 (2005).
36. Hou, B. *et al.* Selective utilization of Toll-like receptor and MyD88 signaling in B cells for enhancement of the antiviral germinal center response. *Immunity* **34,** 375–384 (2011).
37. Rousset, F. *et al.* Interleukin 10 is a potent growth and differentiation factor for activated human B lymphocytes. *Proc. Natl Acad. Sci. USA* **89,** 1890–1893 (1992).
38. Defrance, T. *et al.* Interleukin 10 and transforming growth factor beta cooperate to induce anti-CD40-activated naive human B cells to secrete immunoglobulin A. *J. Exp. Med.* **175,** 671–682 (1992).
39. Punnonen, J. *et al.* Soluble and membrane-bound forms of signaling lymphocytic activation molecule (SLAM) induce proliferation and Ig synthesis by activated human B lymphocytes. *J. Exp. Med.* **185,** 993–1004 (1997).
40. Tokoyoda, K., Hauser, A. E., Nakayama, T. & Radbruch, A. Organization of immunological memory by bone marrow stroma. *Nat. Rev. Immunol.* **10,** 193–200 (2010).
41. Fagarasan, S., Kinoshita, K., Muramatsu, M., Ikuta, K. & Honjo, T. In situ class switching and differentiation to IgA-producing cells in the gut lamina propria. *Nature* **413,** 639–643 (2001).
42. Kang, H. S. *et al.* Signaling via LTbetaR on the lamina propria stromal cells of the gut is required for IgA production. *Nat. Immunol.* **3,** 576–582 (2002).
43. Rakoff-Nahoum, S., Paglino, J., Eslami-Varzaneh, F., Edberg, S. & Medzhitov, R. Recognition of commensal microflora by toll-like receptors is required for intestinal homeostasis. *Cell* **118,** 229–241 (2004).
44. Hiroi, T., Yanagita, M., Ohta, N., Sakaue, G. & Kiyono, H. IL-15 and IL-15 receptor selectively regulate differentiation of common mucosal immune system-independent B-1 cells for IgA responses. *J. Immunol.* **165,** 4329–4337 (2000).

45. Yan, M. *et al.* Identification of a receptor for BLyS demonstrates a crucial role in humoral immunity. *Nat. Immunol.* **1,** 37–41 (2000).
46. Nochi, T. *et al.* Rice-based mucosal vaccine as a global strategy for cold-chain- and needle-free vaccination. *Proc. Natl Acad. Sci. USA* **104,** 10986–10991 (2007).
47. Terahara, K. *et al.* Comprehensive gene expression profiling of Peyer's patch M cells, villous M-like cells, and intestinal epithelial cells. *J. Immunol.* **180,** 7840–7846 (2008).

Acknowledgements

This work was supported by grants from the Program for Promotion of Basic and Applied Research for Innovations in Bio-oriented Industry (BRAIN to J.K.), the Ministry of Education, Culture, Sports, Science and Technology of Japan (Grants-in-Aid for Young Scientists A (22689015 to J.K.), for Scientific Research on Innovative Areas (23116506 to J.K.), for Scientific Research S (23229004 to H.K.), for Scientific Research on Priority Area (19059003 to H.K.), for Challenging Exploratory Research (24659217 to J.K.) and for the Leading-edge Research Infrastructure Program (to J.K. and H.K.)), and the Young Researcher Overseas Visits Program for Vitalizing Brain Circulation (Japan Society for the Promotion of Science) (to J.K., H.K., Y.K. and Y.G.); grants for JSPS Fellows (021-07124 to Y.K.); and grants from the Ministry of Health and Welfare of Japan (J.K. and H.K.), the New Energy and Industrial Technology Development Organization (to H.K.), the Global Center of Excellence Program of the Center of Education and Research for Advanced Genome-based Medicine (to H.K.), the Yakult Bio-Science Foundation (to J.K.) and DK085329 from the National Institute of Diabetes and Digestive and Kidney Diseases (NIDDK, to I.I.).

Author contributions

J.K. planned the research and experiments, analysed data, wrote the paper and directed the research; M.G., E.H., I.I., M.H., Y.S., Y.G., C.P., I.I.I., R.S., L.A., T.W., S.S., Y.K. and S.S. conducted the immunological experiments; K.T. and S.A. provided key materials; and H.K. wrote the paper.

Additional information

Accession codes: Microarray data have been deposited in the National Center for Biotechnology Information Gene Expression Omnibus database under series accession code GSE37225.

Supplementary Information accompanies this paper at http://www.nature.com/naturecommunications

Competing financial interests: The authors declare no competing financial interests.

Reprints and permission information is available online at http://npg.nature.com/reprintsandpermissions/

How to cite this article: Kunisawa, J. *et al.* Microbe-dependent CD11b$^+$ IgA$^+$ plasma cells mediate robust early-phase intestinal IgA responses in mice. *Nat. Commun.* 4:1772 doi: 10.1038/ncomms2718 (2013).

Published June 14, 2013, doi:10.4049/jimmunol.1200636

Critical Role of Dendritic Cells in T Cell Retention in the Interfollicular Region of Peyer's Patches

Takashi Obata,*,[1] Naoko Shibata,*,†,‡,[1] Yoshiyuki Goto,*,§ Izumi Ishikawa,* Shintaro Sato,*,§ Jun Kunisawa,*,†,‡,¶ and Hiroshi Kiyono*,†,§,‖

Peyer's patches (PPs) simultaneously initiate active and quiescent immune responses in the gut. The immunological function is achieved by the rigid regulation of cell distribution and trafficking, but how the cell distribution is maintained remains to be elucidated. In this study, we show that binding of stromal cell–derived lymphoid chemokines to conventional dendritic cells (cDCs) is essential for the retention of naive CD4$^+$ T cells in the interfollicular region (IFR) of PPs. Transitory depletion of CD11c^{high} cDCs in mice rapidly impaired the IFR structure in the PPs without affecting B cell follicles or germinal centers, lymphoid chemokine production from stromal cells, or the immigration of naive T cells into the IFRs of PPs. The cDC-orchestrated retention of naive T cells was mediated by heparinase-sensitive molecules that were expressed on cDCs and bound the lymphoid chemokine CCL21 produced from stromal cells. These data collectively reveal that interactions among cDCs, stromal cells, and naive T cells are necessary for the formation of IFRs in the PPs. *The Journal of Immunology*, **2013, 191: 000–000.**

Intestinal tissue is located in a harsh environment where it is exposed to a complex mixture of external Ags (including digested food materials) and gut microbiota. The gut immune system creates appropriate homeostatic conditions by discriminating between harmful and beneficial Ags (1, 2). Peyer's patches (PPs) are a major GALT that initiates both active and quiescent immune responses in the gastrointestinal tract (3). The PPs share common immunological features with other secondary lymph nodes (LNs), such as the presence of follicular B cell and paraffollicular T cell regions, but they also show unique immunological characteristics that are used to initiate Ag-specific immune responses against Ags from the gut lumen (3). For instance, PPs contain efferent but not afferent lymphatics, therefore decreasing the opportunity for Ags to be delivered to the PPs via the systemic route. Instead, PPs are covered by follicle-associated epithelium, where Ag-sampling M cells transport luminal Ags into the PPs (4). The area under the follicle-associated epithelium is known as the subepithelial dome, an area where dendritic cells (DCs) are present in abundance and function to capture and process the luminal Ags initially taken up by M cells (5).

PP organogenesis begins embryonically with an immunological interaction between lymphoid-lineage retinoic acid–related orphan receptor γt$^+$IL-7R$^+$CD3$^-$CD4$^+$CD45$^+$ PP inducer cells and mesenchymal-lineage VCAM-1$^+$ICAM-1$^+$ PP organizer cells (6). Binding of lymphotoxin (LT) $\alpha_1\beta_2$ on PP inducer cells to its receptor (LTβR) on PP organizer cells results in the production of lymphoid chemokines (e.g., CXCL13, CCL19, and CCL21) from PP organizer cells. These chemokines recruit T cells, B cells, and DCs into the PPs, leading to the subsequent organization of the immunological microarchitecture of the T cell–rich interfollicular region (IFR) and B cell–rich follicles (6). This architecture enables the efficient induction of Ag-specific immune responses against luminal Ags. Formation of cell clusters of DCs, T cells, and B cells in the PPs leads to the induction and activation of Ag-specific lymphocytes together with the expression of gut-homing molecules such as $\alpha_4\beta_7$ integrin and CCR9 (7, 8). Furthermore, the cellular network creates an optimal molecular and cellular environment for promoting μ-to-α class switch recombination of B cells in the germinal centers (9).

DCs are generally known as Ag processing and presenting cells, but several lines of evidence have recently demonstrated that they are also involved in the maintenance of lymphoid structure in the induced BALT (iBALT) and peripheral LNs (10–12); however, how DCs are involved in the formation of the lymphoid structure of PPs is still obscure. In this study, we show that conventional DCs (cDCs) can bind CCL21 on their surface and retain naive CD4$^+$ T cells in the IFRs of PPs.

*Division of Mucosal Immunology, The Institute of Medical Science, The University of Tokyo, Tokyo 108-8639, Japan; †Department of Medical Genome Science, Graduate School of Frontier Science, The University of Tokyo, Tokyo 108-8639, Japan; ‡Laboratory of Vaccine Materials, National Institute of Biomedical Innovation, Osaka 567-0085, Japan; §Core Research for Evolutional Science and Technology, Japan Science and Technology Agency, Tokyo 102-0075, Japan; ¶Graduate School of Pharmaceutical Sciences, Osaka University, Osaka 565-0871, Japan; and ‖Graduate School of Medicine, The University of Tokyo, Tokyo 113-0033, Japan

[1]T.O. and N.S. contributed equally to this work and therefore share the authorship.

Received for publication February 22, 2012. Accepted for publication May 13, 2013.

This work was supported by grants from the Ministry of Education, Culture, Sports, Science and Technology of Japan (for Scientific Research on Innovative Areas [to J.K.], for Scientific Research [to H.K.], for Challenging Exploratory Research [to J.K.], and for the Leading-Edge Research Infrastructure Program [to J.K. and H.K.]), as well as the Young Researcher Overseas Visits Program for Vitalizing Brain Circulation initiated by the Japan Society for the Promotion of Science (to J.K., H.K., and Y.G.). This work was also supported by grants from the Japan Society for the Promotion of Science Fellows (to N.S.), grants from the Ministry of Health and Welfare of Japan (to J.K. and H.K.), the Global Center of Excellence Program of the Center of Education and Research for Advanced Genome-Based Medicine (to H.K.), the Program for Promotion of Basic and Applied Research for Innovations in Bio-Oriented Industry (to J.K.), and by the Yakult Bio-Science Foundation (to J.K.).

Address correspondence and reprint requests to Dr. Jun Kunisawa and Dr. Hiroshi Kiyono, Division of Mucosal Immunology, Department of Microbiology and Immunology, The Institute of Medical Science, The University of Tokyo, 4-6-1 Shirokanedai, Minato-ku, Tokyo 108-8639, Japan. E-mail addresses: kunisawa@ims.u-tokyo.ac.jp (J.K.) and kiyono@ims.u-tokyo.ac.jp (H.K.)

The online version of this article contains supplemental material.

Abbreviations used in this article: BM, bone marrow; cDC, conventional dendritic cell; DC, dendritic cell; DT, diphtheria toxin; DTR, diphtheria toxin receptor; HEV, high endothelial venule; iBALT, inducible BALT; IFR, interfollicular region; LN, lymph node; LT, lymphotoxin; MLN, mesenteric lymph node; pDC, plasmacytoid dendritic cell; PNA, peanut agglutinin; PP, Peyer's patch; Tg, transgenic; WT, wild-type.

www.jimmunol.org/cgi/doi/10.4049/jimmunol.1200636

Materials and Methods

Mice and in vivo treatment

BALB/c mice were purchased from Japan Clea (Tokyo, Japan). CD11c-diphtheria toxin receptor (DTR) transgenic (Tg) mice (13) and CD11b-DTR Tg mice (14) were obtained from The Jackson Laboratory (Bar Harbor, ME). Paucity of LN T cells (*plt/plt*) mice on a BALB/c background were provided by Drs. H. Nakano and T. Kakiuchi (Department of Immunology, Toho University School of Medicine, Tokyo, Japan) (15). For the depletion of DCs and $CD11b^+$ cells, mice were i.p. injected with 500 ng DT dissolved in PBS (Sigma-Aldrich, St. Louis, MO). Bone marrow (BM)-chimeric mice were established by i.v. transfer of 1×10^7 BM cells into irradiated recipient mice. The recipient mice were rested for 8 wk before use. For the heparinase treatment, mice received an i.v. injection of heparinase mixture (heparitinase and heparinase, 1 U each; Seikagaku, Tokyo, Japan) 16 h before analysis (16). As a control, 1 U chondroitinase ABC (Seikagaku) was similarly injected. Mice were maintained under specific pathogen-free conditions at The Institute of Medical Science (The University of Tokyo), and all experiments were conducted in accordance with the guidelines of the Animal Care and Use Committees of The University of Tokyo.

Cell preparation

For the preparation of mononuclear cells from PPs, a standard physical and enzymatic dissociation protocol was employed as previously described (17). Briefly, PP segments were dissected and agitated vigorously in RPMI 1640 containing 0.5 mM EDTA and 2% FCS to remove epithelial cells. The segments were then agitated in RPMI 1640 containing 2% FCS and 0.5 mg/ml collagenase type IV (Wako Chemicals, Osaka, Japan). Similarly, cells were isolated from the mesenteric LNs (MLNs) by agitation with collagenase type IV.

Flow cytometry and cell sorting

Flow cytometry and cell sorting were performed with FACSCanto II and FACSAria (BD Biosciences, San Diego, CA), respectively, as previously described (18). Briefly, cells were first preincubated with an anti-CD16/CD32 mAb (2.4G2; BD Biosciences) and then stained with fluorescently labeled Abs specific for B220, CD3, CD4, CD8α, CD11b, CD11c, CD31, CD45, CD45RB, CD62L, CD69, or PD1 (all from BD Biosciences), or for FR4 (BioLegend, San Diego, CA). For the detection of peanut agglutinin (PNA), cells were reacted with biotinylated PNA (Vector Laboratories, Burlingame, CA) and subsequently incubated with fluorescently labeled streptavidin. Via-Probe (BD Biosciences) was used to discriminate between dead and living cells.

For the detection of surface binding of CCL21, cells were incubated for 10 min with 1 μg/ml CCL21 (PeproTech, Princeton, NJ). After two washes, the cells were reacted with a purified Ab specific for CCL21 (R&D Systems, Minneapolis, MN) followed by additional incubation with a fluorescently labeled goat IgG-specific Ab. For the heparinase treatment, cells were incubated with 25 mU/ml heparinase mixture for 1 h at 37°C (16). All data were analyzed by using FlowJo software (Tree Star, Ashland, OR).

Immunohistochemistry

PPs, MLNs, and spleens were fixed in 4% paraformaldehyde for 15 h at 4°C, washed, and treated in 20% sucrose for 12 h at 4°C. The tissues were embedded in OCT compound (Sakura Finetek Japan, Tokyo, Japan). Sections were stained with appropriate Abs and the tyramide signal amplification system (PerkinElmer, Shelton, CT) (17). Briefly, cryostat sections (7 μm) were treated with 1% H_2O_2 and an avidin/biotin blocking kit (Vector Laboratories) to quench endogenous peroxidase and biotin. After being blocked with anti-CD16/CD32 Ab in TNT buffer (0.1 M Tris-HCl [pH 7.5], 0.15 M NaCl, 0.05% Tween 20) for 15 min at room temperature, sections were stained with a PE-labeled anti-B220 mAb, biotinylated anti-CD11c mAb, biotinylated anti-CD4 mAb (BD Biosciences), purified anti–reticular fibroblast mAb (ER-TR7; BMA Biomedicals, Augst, Switzerland), fluorescein-conjugated PNA (Vector Laboratories), or purified anti–LYVE-1 polyclonal Ab (R&D Systems). For the detection of ER-TR7 and LYVE-1, the sections were additionally incubated with biotinylated secondary Abs (Jackson ImmunoResearch, West Grove, PA). After washes with TNT buffer, the sections were incubated with HRP-conjugated streptavidin (Pierce, Rockford, IL) for 30 min at 4°C, and the fluorescent signal was amplified by using the tyramide signal amplification system with an appropriate fluorescent dye. After the specimens were stained with DAPI (Sigma-Aldrich), they were analyzed by using a confocal laser-scanning microscope (TCS SP2; Leica, Wetzlar, Germany).

Macro-confocal analysis

$CD4^+$ T cells or purified $CD62L^{high}$ naive T cells (1×10^7) were isolated from PPs and MLNs, labeled with 5 μM CFSE (Invitrogen), and adoptively transferred into recipient mice. A macroscopic view of PPs was obtained by using a macro-confocal microscope (AZ-C1; Nikon, Tokyo, Japan).

Quantitative RT-PCR

Total RNA was isolated with TRIzol reagent (Invitrogen), and cDNA was synthesized from the RNA by using a SuperScript VILO cDNA synthesis kit (Invitrogen). Quantitative RT-PCR was performed with the LightCycler system (Roche Diagnostics, Basel, Switzerland) as reported previously (18). The primers and hybrid probes used for the RT-PCR were as follows: CCL19-specific oligonucleotide primers (sense, 5′-GCCAAGAACAAAGGCAACA-3′, antisense, 5′-CACACTCACATCGACTCTCTA-3′), an FITC-labeled probe for CCL19 detection (5′-TGGCCCAGGAAACCAAGGACCA-3′), and a LightCycler Red 640–labeled hybrid probe (5′-AAGAGAGGACCAGGCCTCCT-3′); CCL21-specific oligonucleotide primers (sense, 5′-ACAGACACAGCCCTCAA-3′, antisense, 5′-CATGAGGTGGCTGCTTT-3′), an FITC-labeled probe for CCL21 detection (5′-CCAGGAGATCCCCCACGAACTTC-3′), and a LightCycler Red 640–labeled hybrid probe (5′-AGCTGGGTGGTTCACGGT-3′); GAPDH-specific oligonucleotide primers (sense, 5′-TGAACGGGAAGCTCACTGG-3′, antisense, 5′-TCCACCACCCTGTTGCTGTA-3′), an FITC-labeled probe for GAPDH detection (5′-CTGAGGACCAGGTTGTCTCCTGCGA-3′), and a LightCycler Red 640–labeled hybrid probe (5′-TTCAACAGCAACTCCCACTCTTCCACC-3′) (Nihon Gene Research Laboratories, Sendai, Japan).

Statistical analyses

The results were compared using the Student *t* test. The threshold for statistical significance was set at $p < 0.05$.

Results

Depletion of cDCs disrupts T cell regions in the IFR of PPs

To examine the involvement of DCs in the maintenance of PP microarchitecture, we employed a CD11c-DTR Tg mouse system (13). A previous study demonstrated that a single injection of DT into these Tg mice ablated DCs expressing high levels of CD11c in vivo (13, 19). We initially tested whether DT treatment would induce a similar reduction of DCs in the intestinal tissues. We found that the i.p. injection of high amounts of DT (25 ng/g body weight) into CD11c-DTR Tg mice depleted $CD11c^{high}$ cDCs in the PPs, but not $CD11c^{int}B220^+$ plasmacytoid DCs (pDCs) 24 h after the injection (Fig. 1A, 1B). Immunohistochemical analysis indicated that cDCs were depleted in both the subepithelial dome and IFR of the PPs (Fig. 1C). DT treatment did not affect the DC population in wild-type (WT) mice (Supplemental Fig. 2G).

Depletion of cDCs decreases naive $CD4^+$ T cells in the PPs

The depletion of cDCs in CD11c-DTR Tg mice by DT treatment was associated with a small reduction of the T cell population. Indeed, flow cytometric analysis showed that the number of $CD3^+$ T cells decreased in the PPs of CD11c-DTR Tg mice receiving DT. Although PNA^+ germinal center B cells were decreased, presumably due to the lack of Ag presentation by cDCs, $B220^+$ B cells and the germinal center distribution were retained (Supplemental Fig. 1A–C). Among $CD3^+$ T cell populations, $CD4^+$ T cells, the dominant T cell population in the PPs, and especially naive $CD4^+$ cells expressing high levels of CD62L and CD45RB were decreased by the DT treatment (Fig. 2A–C, Supplemental Fig. 1D). In contrast, $CD69^+$ activated T cells, $FR4^+$ regulatory T cells, and $PD1^+$ follicular helper T cells were not affected by the DT treatment (Fig. 2B–E).

Consistent with the fact that naive $CD4^+$ T cells are predominantly located in the IFR of PPs (3), immunohistochemical analysis revealed that the IFR structure was disrupted in cDC-depleted mice (Fig. 2F). To examine the T cell distribution at the tissue

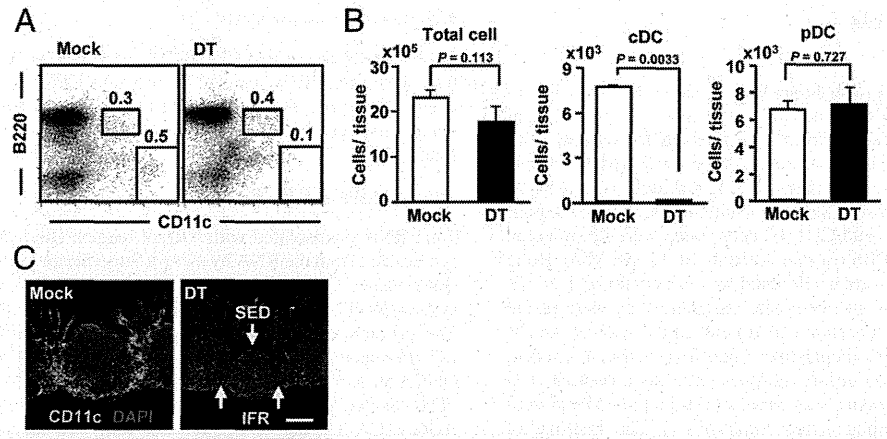

FIGURE 1. Depletion of cDCs in the PPs of CD11c-DTR Tg mice by DT treatment. (**A**) CD11c-DTR Tg mice were given an i.p. injection of DT (*right*) or PBS (mock, *left*). After 24 h, cells were isolated from the PPs for the flow cytometric analysis of CD11c and B220. Data are representative of three independent experiments (three mice per group for each experiment). (**B**) The cell numbers of cDCs (*top*) and pDCs (*bottom*) were calculated from the total cell numbers and cell ratios determined with flow cytometry (n = 3/group; similar results were obtained from three separate experiments). (**C**) Confocal microscopic analysis of the PPs was performed using a CD11c-specific Ab (green) and DAPI (blue) for counterstaining. Data are representative of three independent experiments (three mice per group for each experiment). Scale bar, 300 μm. SED, Subepithelial dome.

level, we employed macro-confocal microscopy (20). When CFSE-labeled CD62L^{high} naive T cells were adoptively transferred into WT mice, T cells accumulated in the IFR of PPs and reached the steady-state 15 h after the transfer. As we previously reported (20), the mesh-like structure of the T cell area was clearly detected in the IFR of PPs (Fig. 2G, mock). Administration of DT to CD11c-DTR Tg mice resulted in the disruption of IFRs throughout the PPs (Fig. 2G, DT). In contrast, T cells were preferentially observed in the follicular area in the PPs of DC-depleted mice (Fig. 2F, 2G). Because cDCs recovered 144 h after the single DT injection, and the disrupted T cell regions and the number of naive T cells were restored with the recovery of cDCs (Fig. 2H, 2I), it seems that the depletion of cDCs was temporary and reversible and the distribution of T cells in the IFR depends on the presence of cDCs.

To exclude the possibility that DT affected nonhematopoietic cells and therefore removed cDCs through an indirect mechanism, we made BM-chimeric mice. Eight weeks after BM transfer from CD11c-DTR Tg mice into irradiated WT mice, the reconstituted WT mice were given DT i.p. These mice also showed depletion of cDCs (Supplemental Fig. 2A) and aberrant T cell organization in the IFR, with a decrease of naive T cells and comparable levels of FR4$^+$ regulatory T cells and PD1$^+$ follicular helper T cells (Supplemental Fig. 2B–D). Additionally, T cells barely expressed CD11c in the PPs (unpublished data), and B220$^+$ cells, including CD11c$^+$ pDCs and CD11c$^-$ B cells, were not affected by the DT treatment (Fig. 1A). To avoid the possibility that excess inflammation induced by cell death might have disrupted the T cell distribution, we analyzed CD11b-DTR Tg mice and confirmed that treatment of CD11b-DTR Tg mice with DT did not affect the distribution of T cells in the PPs (Supplemental Fig. 2E). Together with a previous report that PP structure was maintained in the absence of RET$^+$CD3$^-$CD4$^-$IL-7Rα$^-$CD11c$^+$ cells, which are key regulatory cells in PP organogenesis and are also susceptible to DT (21, 22), our data collectively indicate that the structure of the IFR with regard to T cells is mediated by cDCs.

We then examined whether the rapid disruption of T cell regions by temporary cDC depletion is specific to PPs or is a more general phenomenon in secondary LNs by investigating MLNs, which drain to PPs, the intestinal lamina propria, and the spleen. The DT treatment barely affected the T cell regions or the number of naive T cells in the MLNs and spleens, despite depletion of the DCs (Supplemental Fig. 3 and unpublished data), as had been previously reported (19, 23). Taken together, these data suggest that the rapid disruption of the T cell regions by the cDC deletion was specific to the IFRs of PPs.

Depletion of cDCs affects T cell retention in, but not immigration into, the PPs

We next examined whether the disruption of IFR T cells by the cDC deletion was due to the inhibition of T cell immigration, retention, or both. We performed macro-confocal imaging in individual mice to observe the distribution of adoptively transferred CD4$^+$ T cells in PPs over time. In this experimental condition, we focused on the surface of PPs to predominantly show images of naive T cells. When CD4$^+$ T cells labeled with CFSE were adoptively transferred into mice, the labeled CD4$^+$ T cells rapidly immigrated into PPs and gradually accumulated in the IFRs; cell motility and accumulation as well as the number of CFSE$^+$ naive T cells and activated T cells in the PPs were similar in the cDC-depleted and mock-treated mice (Fig. 3A). Consistent with the normal immigration of CD4$^+$ T cells into PPs, LYVE-1$^+$ high endothelial venules (HEVs), a portal site for lymphocyte entry into the PPs, developed normally in the cDC-depleted mice (Fig. 3B).

We then examined the effect of cDC depletion on T cell retention in the IFR of PPs. As mentioned above, T cell accumulation in the IFR of PPs reached the steady-state 15 h after the adoptive transfer. Indeed, a clear T cell region was detected in the IFR of PPs (Fig. 3C). When DT was administered to CD11c-DTR Tg mice 15 h after the adoptive transfer, the IFR structure almost disappeared, and the number of CFSE$^+$ naive T cells in PPs, but not activated T cells, had also decreased 8 h after the DT treatment (Fig. 3C). In contrast, the IFR structure remained normal in the PPs of CD11c-DTR Tg mice without the DT treatment (Fig. 3C). These data indicate that cDCs are specifically involved in T cell retention in the IFR of PPs, but do not affect their immigration into the tissue.

Stromal cells reside normally in the IFR of PPs and produce CCL19 and CCL21 in cDC-depleted mice

Stromal cells in the LNs are thought to play an essential role in the regulation of T cell motility by producing lymphoid chemokines (e.g., CCL19 and CCL21) (15, 24). Consistent with this, we found a disruption of IFR T cells and a decrease of naive CD4$^+$ T cells in

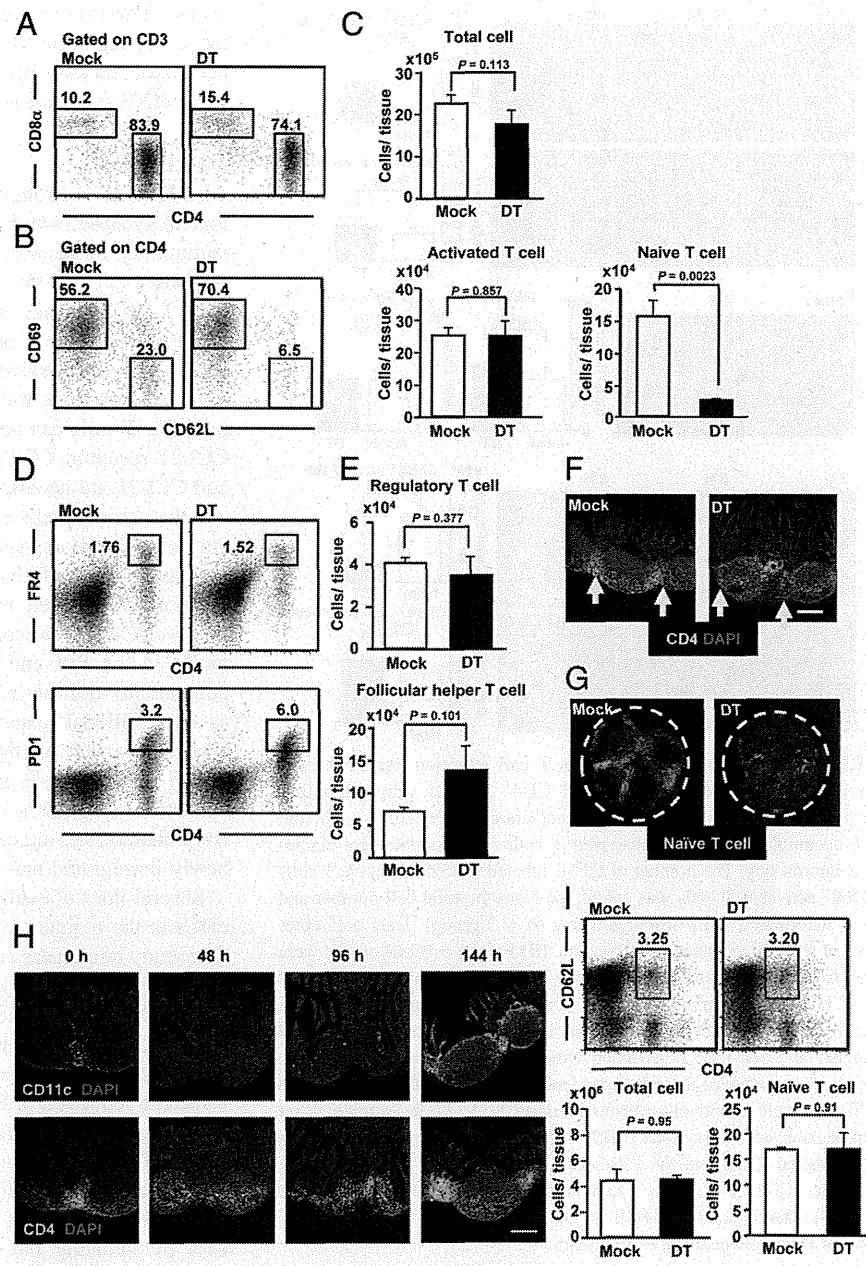

FIGURE 2. Selective reduction of naive $CD4^+$ T cells in the IFRs of PPs by cDC depletion. (**A** and **B**) Flow cytometric analysis was performed 24 h after a DT injection using Abs specific for CD3, CD4, CD8α, CD62L, and CD69. Data are representative of three independent experiments (three mice per group in one experiment). (**C** and **E**) Cells were isolated from one PP and the number of each cells of each type was calculated from the total cell numbers and cell ratios determined with flow cytometry (n = 3/group). Data are representative of three independent experiments. (**D**) Cells were isolated from the PPs for the flow cytometric analysis of CD4 and FR4 (*top*) or PD1 (*bottom*) expression (n = 3/group). Similar results were obtained from three independent experiments. (**F**) Frozen sections of PPs were stained with an Ab specific for CD4 (green) and DAPI (blue). The arrows point to IFRs (n = 3/group). Data are representative of three independent experiments. (**G**) Fifteen hours after the adoptive transfer of CFSE-labeled $CD62L^{high}$ naive T cells into CD11c-DTR Tg mice, the mice were treated with DT. Eight hours after the DT injection, the T cell distribution in the PPs was examined with macro-confocal microscopy. The dotted white lines represent the edges of the PPs. Data are representative of three independent experiments (n = 3/group). (**H**) CD11c-DTR Tg mice received a DT injection. After 0, 48, 96, or 144 h, the animals were sacrificed and frozen sections of PPs were stained with an Ab for CD11c (*top*) or CD4 (*bottom*) together with DAPI (n = 3/group). Data are representative of three independent experiments. (**I**) Flow cytometric analysis was performed 144 h after a DT injection using Abs specific for CD4 and CD62L (*top*). Cells were isolated from one PP and the number of each cells of each type was calculated from the total cell numbers and cell ratios determined with flow cytometry (bottom) (n = 3/group). Data are representative of three independent experiments. Scale bars in (F) and (H), 300 μm.

plt/plt mice, which lack functional CCL19 and CCL21 (Fig. 4A, 4B). Thus, it was possible that cDC depletion affected stromal cells, including their synthesis of chemokines, and thus indirectly induced the disorganized structure of IFR T cell regions in the PPs. To test this possibility, we examined stromal cells in the PPs of CD11c-DTR Tg mice after the DT treatment. Histological and flow cytometric analysis revealed that ER-$TR7^+CD45^-$ stromal cells were present normally at the IFR of PPs of cDC-depleted mice (Fig. 4C, 4D).

We then measured the expression of lymphoid chemokines (CCL19 and CCL21) by stromal cells. We purified $CD45^-$ stromal cells and examined the expression of CCL19 and CCL21 by quantitative RT-PCR. No significant differences were observed between cDC-deleted and intact mice in expression of either CCL19 or CCL21 (Fig. 4E). Taken together, these results suggest that CCL19 and CCL21 are essential for the maintenance of the IFR, but the disorganized IFR in cDC-depleted mice was not due to a disruption in the localization and function of stromal cells.

CCL21 bound to cDCs plays a pivotal role in the maintenance of IFR T cell regions in the PPs

It was previously reported that DCs, as well as stromal cells, produce CCL19 (25). We therefore hypothesized that CCL19 and CCL21 from cDCs play a major role in the localization of T cells in IFR of PPs. To test this hypothesis, we made two types of BM-chimeric mice; in one, irradiated WT mice received adoptive transfer of BM cells from *plt/plt* mice, and in the other, the adoptive transfer was from WT mice to *plt/plt* mice. Normal localization of T cells was noted in the IFRs of PPs in mice lacking the production of CCL19 and CCL21 from hematopoietic cells, including cDCs, whereas disrupted T cell regions were observed in the PPs of BM-chimeric *plt/plt* mice that had received WT BM cells (Fig. 5A). We cannot completely exclude the possibility that endogenous cDCs are retained in BM-chimeric mice. However, if the endogenous cDCs retained $CD4^+$ T cells through the expression of CCL19 and CCL21, we would detect $CD4^+$ T cell retention in both WT mice receiving *plt/plt* BM cells and *plt/plt* mice receiving WT BM cells. In fact,

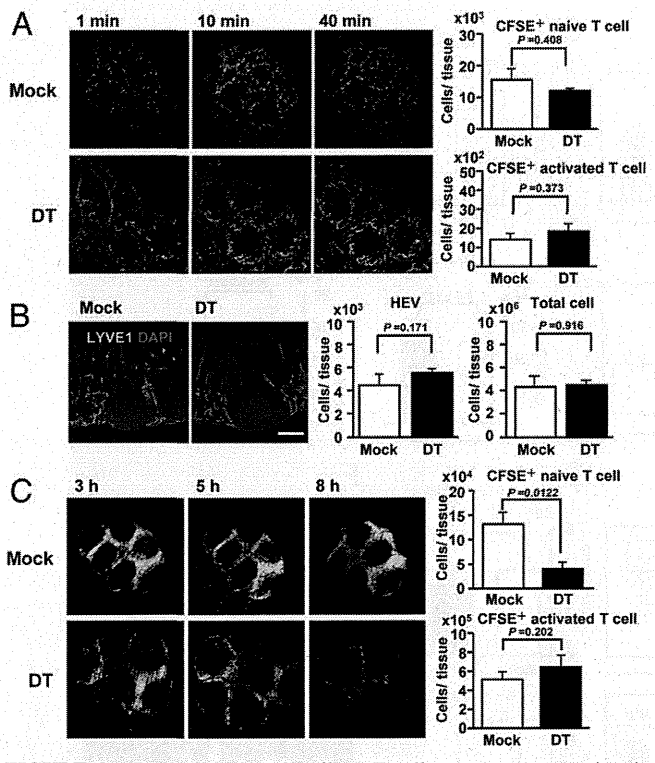

FIGURE 3. Depletion of cDCs affects T cell retention, but not immigration into the PPs. (**A**) CFSE-labeled $CD4^+$ T cells were adoptively transferred into cDC-depleted (DT) or intact (mock) mice. After 1, 10, and 40 min, accumulation of the transferred T cells was examined by macro-confocal microscopy. The number of CFSE-labeled $CD62L^{high}$ naive T cells and $CD69^+$ activated T cells was calculated from the total cell number and cell ratio determined with flow cytometry (n = 3/group). Data are representative of three independent experiments. (**B**) Frozen sections of PPs were prepared from cDC-depleted (DT) and intact (mock) mice for the staining of LYVE-1^+ HEVs and efferent lymphatic vessels (green). Scale bar, 300 μm. The number of $CD31^-CD45^+$ endothelial cells was calculated from the total cell number and cell ratio determined with flow cytometry (n = 3/group). Data are representative of three independent experiments. (**C**) CFSE-labeled $CD4^+$ T cells were adoptively transferred into CD11c-DTR Tg mice. After 15 h, mice received DT or mock (PBS) treatment. Macroscopic distribution of CFSE-labeled T cells in the PPs was examined at the indicated times. CFSE-labeled $CD62L^{high}$ naive T cells and $CD69^+$ activated T cells were counted 8 h after injection of PBS or DT (n = 3/group). Data are representative of three independent experiments.

only WT mice receiving *plt/plt* BM cells had a normal T cell area, whereas *plt/plt* mice receiving WT BM cells showed an impaired T cell area. These findings indicate that, although both cDCs and CCL19/21 are involved in the maintenance of $CD4^+$ T cells in the IFRs of PPs, CCL19 and CCL21 expressed by cDCs are not sufficient to retain $CD4^+$ T cells in the PPs.

Several lines of evidence have demonstrated that chemokines bound to the cell surface can mediate cell motility in vivo (26). Thus, we hypothesized that exogenous CCL19 and CCL21 bound to the surface of cDCs regulate T cell retention. We found that cDCs can bind CCL21 on the cell surface, whereas $CD4^+$ T cells barely bound to CCL21 (Fig. 5B).

Heparan sulfate is a glycosaminoglycan that binds to chemokines in vivo (13). We found that treatment with a heparinase mixture inhibited the binding of CCL21 to the cDCs (Fig. 5C). These findings allowed us to examine the role of heparan sulfate in T cell retention in vivo. As with cDC depletion, treatment of the WT mice with the heparinase mixture led to the disruption of $CD4^+$ T cells and the decrease of naive T cells, whereas chondroitinase ABC, another enzyme that degrades glycosaminoglycans, did not affect the T cell region in the PPs (Fig. 5D). We also confirmed that the heparinase mixture had no additional effect on the IFR structure when cDCs were already depleted (Supplemental Fig. 4).

Discussion

As APCs, DCs strongly adhere to T cells through the immunological synapse, which includes the MHC/TCR complex and costimulatory molecules; this adhesion primes Ag-specific T cell responses (27). In this study, we showed that cDCs also interact with T cells through an immobilized chemokine, CCL21. This chemokine-mediated interaction is required for the retention of T cells, especially naive T cells, in the IFR of PPs, a key organized inductive tissue for the gut immune system. This selective effect on naive T cells can be explained by their high expression of the CCL21 receptor, CCR7. It was previously reported that CCL19 and CCL21 are necessary for the maintenance of IFRs in the PPs and that stromal cells are important in this pathway (15, 24). Our current findings suggest that stromal and T cell interactions are not sufficient, and that DCs are additionally required for the chemokine-mediated maintenance of the IFR structure of PPs. In the cDC-depleted condition, stromal cells were distributed normally in the PPs and expressed levels of CCL19 and CCL21 comparable to those in mice with intact cDCs. Although DCs act as an additional source of CCL19 (25), our experiment using adoptive transfer of BM cells from *plt/plt* mice indicated that the T cell region defects in the IFR were not due to production of chemokines by cDCs. Thus, it is plausible that stromal cell–derived chemokines are captured by cDCs and are then used to retain newly immigrated naive T cells in the IFRs of PPs.

Several lines of evidence have demonstrated the involvement of cDCs in the maintenance of secondary and tertiary LNs (10–12). One study demonstrated that cDCs play a major role in providing an LT signal for the promotion of lymphoid chemokines, especially CXCL13; depletion of cDCs led to the disintegration of the iBALT formed by influenza infection (11). Because CXCL13 recruits mainly B cells (28), these defects were associated with a specific reduction of B cells in the iBALT (11). In contrast to the function of cDCs in iBALT formation, our study demonstrated that cDCs are involved in the retention of T cells in the IFRs without affecting B cell follicles or the germinal center. Another study recently showed that cDCs control lymphocyte entry into LNs by inducing the expression of HEV-associated molecules (e.g., FucT-VII, GlcNAc6ST-2, and the L-selectin counterreceptor GLYCAM1) (12). This study showed that DCs expressing LT directly interacted with HEVs expressing LTβ receptors to induce these molecules. Indeed, impaired lymphocyte migration into the LN in cDC-depleted mice was restored by the adoptive transfer of LT-sufficient, but not LT-deficient, DCs. Of note, the phenotypes were observed in the brachial, inguinal, and cervical LNs, but not PPs (12). Additionally, unlike in our experiments, long-term treatment of CD11c-DTR mice with DT (~8 d) was required to observe these phenotypes. Another study recently reported that semimature DCs reached LNs via the afferent lymph, which is also involved in the T cell homeostasis in the LN (29). They showed that semimature DCs produce vascular endothelial growth factor, which induces the growth and differentiation of HEVs and efficient homing of T cells to LNs. They also showed that semimature DCs not only promote the production of CCL21 from stromal cells but also bind CCL21 via the heparin-binding domain (29). Our study demonstrated that HEVs developed normally in the cDC-depleted mice, and cDCs did not increase the expression of CCL21 from stromal cells, indicating that semimature DCs and

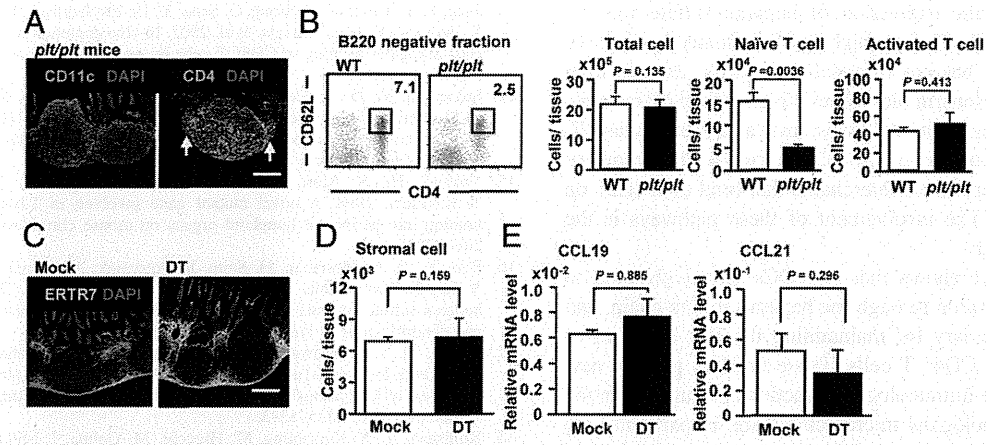

FIGURE 4. Presence of stromal cells expressing CCL19 and CCL21 in the IFRs of cDC-depleted mice. (**A**) Frozen sections of PPs were prepared from *plt/plt* mice for the staining of CD4 (*right*) and CD11c (*left*) (both shown in green). The arrows point to IFRs (n = 3/group). Data are representative of three independent experiments. (**B**) Cells were isolated from the PPs for the flow cytometric analysis of CD4 and CD62L expression, and the number of $CD62L^{high}$ naive T cells and $CD69^{+}$ activated T cells was calculated (n = 3/group). Data are representative of three independent experiments. (**C**) Frozen sections of PPs were prepared from cDC-depleted (DT) and intact (mock) mice for the staining of ER-$TR7^{+}$ stromal cells (green) (n = 3/group). Data are representative of three independent experiments. Scale bar, 300 μm. (**D**) Cells were isolated from one PP and the number of $CD45^{-}$ stromal cells was calculated from the total cell number and cell ratio determined with flow cytometry (n = 3/group). Data are representative of three independent experiments. (**E**) Quantitative RT-PCR analysis of CCL19 and CCL21 expression on stromal cells from the PPs of cDC-depleted (DT) and intact (mock) mice. The data are presented as the ratio to GAPDH mRNA (mean ± SD, n = 4). Data are representative of three independent experiments.

cDCs regulate T cell distribution in different ways. These findings suggest that PP cDCs have a unique function in regulating T cell retention.

The selective phenotype of PP T cells in cDC-depleted mice could be explained by the sensitive ability of PP DCs to bind CCL21 through the expression of heparin or heparinase-sensitive

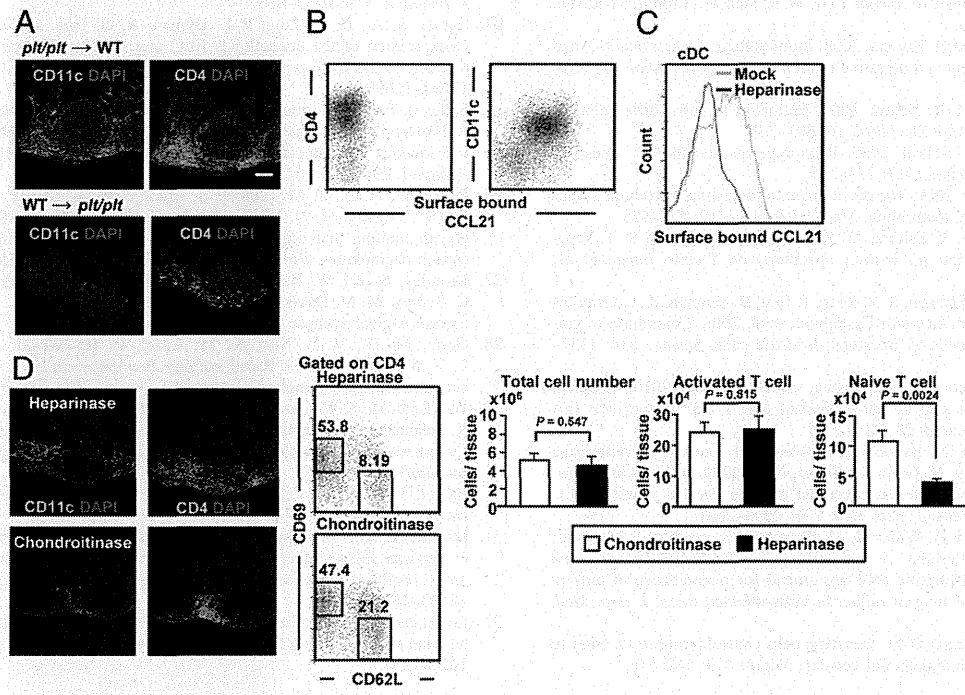

FIGURE 5. cDCs are not the main producers of CCL19 and CCL21, but bind exogenous CCL19 and CCL21. (**A**) PP tissue sections were prepared from irradiated WT mice receiving BM cells from *plt/plt* mice (*top*) or vice versa (*bottom*). PP sections were stained with Abs for CD11c (*left*) and CD4 (*right*) (n = 3/group). Data are representative of three independent experiments. Scale bar, 300 μm. (**B**) Sorted $CD4^{+}$ T cells (*left*) and cDCs (*right*) from PPs were preincubated for 10 min with 1 μg/ml CCL21 and then incubated with a purified goat Ab specific for CCL21. The cells were then stained with fluorescently labeled Abs specific for goat IgG, CD4, and CD11c and subjected to flow cytometry (n = 3 per group). Data are representative of three independent experiments. (**C**) Sorted heparinase- (black) or mock-treated (blue) cDCs from PPs were preincubated for 10 min with 1 μg/ml CCL21 and then incubated with a purified goat Ab specific for CCL21. The cells were then stained with fluorescently labeled Abs specific for goat IgG and subjected to flow cytometry (n = 3/group). Data are representative of three independent experiments. (**D**) WT mice received an i.v. injection of heparinase mixture (heparitinase and heparinase, 1 U each) or 1 U chondroitinase ABC. After 16 h, PP tissue sections were prepared for the staining of CD11c (*left*) and CD4 (*right*). Cells were isolated from the PPs for the flow cytometric analysis of CD4 and CD62L expression (*upper right*). Cells were isolated from one PP and the number of $CD62L^{high}$ naive T cells and $CD69^{+}$ activated T cells was calculated from the total cell number and cell ratio determined with flow cytometry (n = 3/group). Data are representative of three independent experiments.

molecules. Subset-specific expression of heparan sulfate was reported in mast cells (30). Indeed, highly differentiated connective tissue–type mast cells, but not mucosal mast cells, express high levels of heparin (30). Heparin biosynthesis is mediated by multiple complex steps involving many enzymes such as *N*-deacetylase/*N*-sulfotransferase and exostoses-1 (31, 32). Exostoses-1 is required for the formation of heparan sulfate chains that bind to CCL21 on endothelial cells (16). The involvement of these pathways is the subject of our next study.

In summary, we have shown that PP cDCs sensitively bind to CCL21 at low concentration through the heparan sulfate chain, and this interaction is necessary for maintaining the IFR structure of PPs by retaining naive $CD4^+$ T cells. These findings provide new evidence for the unique immunological functions of gut DCs in the maintenance of immunological microarchitecture, in particular the IFR of the PP, a key organized lymphoid structure in the gut immune system.

Acknowledgments

We thank Dr. T. Okada (RIKEN Research Center for Allergy and Immunology, Yokohama, Japan) for helpful discussions.

Disclosures

The authors have no financial conflicts of interest.

References

1. Hill, D. A., and D. Artis. 2010. Intestinal bacteria and the regulation of immune cell homeostasis. *Annu. Rev. Immunol.* 28: 623–667.
2. Kiyono, H., J. Kunisawa, J. R. McGhee, and J. Mestecky. 2008. The mucosal immune system. In *Fundamental Immunology.* W. E. Paul, ed. Lippincott-Raven, Philadelphia, p. 983–1030.
3. Kunisawa, J., T. Nochi, and H. Kiyono. 2008. Immunological commonalities and distinctions between airway and digestive immunity. *Trends Immunol.* 29: 505–513.
4. Kraehenbuhl, J. P., and M. R. Neutra. 2000. Epithelial M cells: differentiation and function. *Annu. Rev. Cell Dev. Biol.* 16: 301–332.
5. Johansson, C., and B. L. Kelsall. 2005. Phenotype and function of intestinal dendritic cells. *Semin. Immunol.* 17: 284–294.
6. Eberl, G., and M. Lochner. 2009. The development of intestinal lymphoid tissues at the interface of self and microbiota. *Mucosal Immunol.* 2: 478–485.
7. Iwata, M., A. Hirakiyama, Y. Eshima, H. Kagechika, C. Kato, and S. Y. Song. 2004. Retinoic acid imprints gut-homing specificity on T cells. *Immunity* 21: 527–538.
8. Mora, J. R., M. Iwata, B. Eksteen, S. Y. Song, T. Junt, B. Senman, K. L. Otipoby, A. Yokota, H. Takeuchi, P. Ricciardi-Castagnoli, et al. 2006. Generation of gut-homing IgA-secreting B cells by intestinal dendritic cells. *Science* 314: 1157–1160.
9. Fagarasan, S., S. Kawamoto, O. Kanagawa, and K. Suzuki. 2010. Adaptive immune regulation in the gut: T cell-dependent and T cell-independent IgA synthesis. *Annu. Rev. Immunol.* 28: 243–273.
10. Halle, S., H. C. Dujardin, N. Bakocevic, H. Fleige, H. Danzer, S. Willenzon, Y. Suezer, G. Hämmerling, N. Garbi, G. Sutter, et al. 2009. Induced bronchus-associated lymphoid tissue serves as a general priming site for T cells and is maintained by dendritic cells. *J. Exp. Med.* 206: 2593–2601.
11. GeurtsvanKessel, C. H., M. A. Willart, I. M. Bergen, L. S. van Rijt, F. Muskens, D. Elewaut, A. D. Osterhaus, R. Hendriks, G. F. Rimmelzwaan, and B. N. Lambrecht. 2009. Dendritic cells are crucial for maintenance of tertiary lymphoid structures in the lung of influenza virus-infected mice. *J. Exp. Med.* 206: 2339–2349.
12. Moussion, C., and J. P. Girard. 2011. Dendritic cells control lymphocyte entry to lymph nodes through high endothelial venules. *Nature* 479: 542–546.
13. Jung, S., D. Unutmaz, P. Wong, G. Sano, K. De los Santos, T. Sparwasser, S. Wu, S. Vuthoori, K. Ko, F. Zavala, et al. 2002. In vivo depletion of $CD11c^+$ dendritic cells abrogates priming of $CD8^+$ T cells by exogenous cell-associated antigens. *Immunity* 17: 211–220.
14. Stoneman, V., D. Braganza, N. Figg, J. Mercer, R. Lang, M. Goddard, and M. Bennett. 2007. Monocyte/macrophage suppression in CD11b diphtheria toxin receptor transgenic mice differentially affects atherogenesis and established plaques. *Circ. Res.* 100: 884–893.
15. Nakano, H., S. Mori, H. Yonekawa, H. Nariuchi, A. Matsuzawa, and T. Kakiuchi. 1998. A novel mutant gene involved in T-lymphocyte-specific homing into peripheral lymphoid organs on mouse chromosome 4. *Blood* 91: 2886–2895.
16. Bao, X., E. A. Moseman, H. Saito, B. Petryniak, A. Thiriot, S. Hatakeyama, Y. Ito, H. Kawashima, Y. Yamaguchi, J. B. Lowe, et al. 2010. Endothelial heparan sulfate controls chemokine presentation in recruitment of lymphocytes and dendritic cells to lymph nodes. *Immunity* 33: 817–829.
17. Gohda, M., J. Kunisawa, F. Miura, Y. Kagiyama, Y. Kurashima, M. Higuchi, I. Ishikawa, I. Ogahara, and H. Kiyono. 2008. Sphingosine 1-phosphate regulates the egress of IgA plasmablasts from Peyer's patches for intestinal IgA responses. *J. Immunol.* 180: 5335–5343.
18. Kunisawa, J., Y. Kurashima, M. Higuchi, M. Gohda, I. Ishikawa, I. Ogahara, N. Kim, M. Shimizu, and H. Kiyono. 2007. Sphingosine 1-phosphate dependence in the regulation of lymphocyte trafficking to the gut epithelium. *J. Exp. Med.* 204: 2335–2348.
19. Sapoznikov, A., J. A. Fischer, T. Zaft, R. Krauthgamer, A. Dzionek, and S. Jung. 2007. Organ-dependent in vivo priming of naive $CD4^+$, but not $CD8^+$, T cells by plasmacytoid dendritic cells. *J. Exp. Med.* 204: 1923–1933.
20. Kunisawa, J., Y. Kurashima, and H. Kiyono. 2012. Gut-associated lymphoid tissues for the development of oral vaccines. *Adv. Drug Deliv. Rev.* 64: 523–530.
21. Fahlén-Yrlid, L., T. Gustafsson, J. Westlund, A. Holmberg, A. Strömbeck, M. Blomquist, G. G. MacPherson, J. Holmgren, and U. Yrlid. 2009. $CD11c^{high}$ dendritic cells are essential for activation of $CD4^+$ T cells and generation of specific antibodies following mucosal immunization. *J. Immunol.* 183: 5032–5041.
22. Veiga-Fernandes, H., M. C. Coles, K. E. Foster, A. Patel, A. Williams, D. Natarajan, A. Barlow, V. Pachnis, and D. Kioussis. 2007. Tyrosine kinase receptor RET is a key regulator of Peyer's patch organogenesis. *Nature* 446: 547–551.
23. Berndt, B. E., M. Zhang, G. H. Chen, G. B. Huffnagle, and J. Y. Kao. 2007. The role of dendritic cells in the development of acute dextran sulfate sodium colitis. *J. Immunol.* 179: 6255–6262.
24. Luther, S. A., H. L. Tang, P. L. Hyman, A. G. Farr, and J. G. Cyster. 2000. Coexpression of the chemokines ELC and SLC by T zone stromal cells and deletion of the ELC gene in the *plt/plt* mouse. *Proc. Natl. Acad. Sci. USA* 97: 12694–12699.
25. Sallusto, F., B. Palermo, D. Lenig, M. Miettinen, S. Matikainen, I. Julkunen, R. Forster, R. Burgstahler, M. Lipp, and A. Lanzavecchia. 1999. Distinct patterns and kinetics of chemokine production regulate dendritic cell function. *Eur. J. Immunol.* 29: 1617–1625.
26. Proudfoot, A. E., T. M. Handel, Z. Johnson, E. K. Lau, P. LiWang, I. Clark-Lewis, F. Borlat, T. N. Wells, and M. H. Kosco-Vilbois. 2003. Glycosaminoglycan binding and oligomerization are essential for the in vivo activity of certain chemokines. *Proc. Natl. Acad. Sci. USA* 100: 1885–1890.
27. Bromley, S. K., W. R. Burack, K. G. Johnson, K. Somersalo, T. N. Sims, C. Sumen, M. M. Davis, A. S. Shaw, P. M. Allen, and M. L. Dustin. 2001. The immunological synapse. *Annu. Rev. Immunol.* 19: 375–396.
28. Gunn, M. D., V. N. Ngo, K. M. Ansel, E. H. Ekland, J. G. Cyster, and L. T. Williams. 1998. A B-cell-homing chemokine made in lymphoid follicles activates Burkitt's lymphoma receptor-1. *Nature* 391: 799–803.
29. Wendland, M., S. Willenzon, J. Kocks, A. C. Davalos-Misslitz, S. I. Hammerschmidt, K. Schumann, E. Kremmer, M. Sixt, A. Hoffmeyer, O. Pabst, and R. Förster. 2011. Lymph node T cell homeostasis relies on steady state homing of dendritic cells. *Immunity* 35: 945–957.
30. Kolset, S. O., K. Prydz, and G. Pejler. 2004. Intracellular proteoglycans. *Biochem. J.* 379: 217–227.
31. Dagälv, A., K. Holmborn, L. Kjellén, and M. Abrink. 2011. Lowered expression of heparan sulfate/heparin biosynthesis enzyme *N*-deacetylase/*N*-sulfotransferase 1 results in increased sulfation of mast cell heparin. *J. Biol. Chem.* 286: 44433–44440.
32. Lortat-Jacob, H., A. Grosdidier, and A. Imberty. 2002. Structural diversity of heparan sulfate binding domains in chemokines. *Proc. Natl. Acad. Sci. USA* 99: 1229–1234.

IAI
Journals.ASM.org

Nanogel-Based PspA Intranasal Vaccine Prevents Invasive Disease and Nasal Colonization by *Streptococcus pneumoniae*

Il Gyu Kong,[a,b,c] Ayuko Sato,[a,d] Yoshikazu Yuki,[a,d] Tomonori Nochi,[e] Haruko Takahashi,[f] Shinichi Sawada,[f] Mio Mejima,[a] Shiho Kurokawa,[a] Kazunari Okada,[a,d] Shintaro Sato,[a,d] David E. Briles,[g] Jun Kunisawa,[a,d,h,i] Yusuke Inoue,[j] Masafumi Yamamoto,[k] Kazunari Akiyoshi,[f] Hiroshi Kiyono[a,b,d,h]

Division of Mucosal Immunology, Department of Microbiology and Immunology,[a] and International Research and Development Center for Mucosal Vaccines,[h] The Institute of Medical Science, The University of Tokyo, Tokyo, Japan; Graduate School Medicine and Faculty of Medicine, The University of Tokyo, Tokyo, Japan[b]; Department of Otorhinolaryngology, Seoul National University College of Medicine, Seoul, South Korea[c]; Core Research for Evolutional Science and Technology (CREST), Japan Science and Technology Agency, Tokyo, Japan[d]; Division of Infectious Diseases, Center for AIDS Research, University of North Carolina School of Medicine, Chapel Hill, North Carolina, USA[e]; Department of Polymer Chemistry, Kyoto University Graduate School of Engineering, Kyoto, Japan[f]; Department of Microbiology, University of Alabama at Birmingham, Birmingham, Alabama, USA[g]; Laboratory of Vaccine Materials, National Institute of Biomedical Innovation, Osaka, Japan[i]; Department of Diagnostic Radiology, Kitasato University School of Medicine, Kanagawa, Japan[j]; Department of Microbiology and Immunology, Nihon University School of Dentistry at Matsudo, Chiba, Japan[k]

To establish a safer and more effective vaccine against pneumococcal respiratory infections, current knowledge regarding the antigens common among pneumococcal strains and improvements to the system for delivering these antigens across the mucosal barrier must be integrated. We developed a pneumococcal vaccine that combines the advantages of pneumococcal surface protein A (PspA) with a nontoxic intranasal vaccine delivery system based on a nanometer-sized hydrogel (nanogel) consisting of a cationic cholesteryl group-bearing pullulan (cCHP). The efficacy of the nanogel-based PspA nasal vaccine (cCHP-PspA) was tested in murine pneumococcal airway infection models. Intranasal vaccination with cCHP-PspA provided protective immunity against lethal challenge with *Streptococcus pneumoniae* Xen10, reduced colonization and invasion by bacteria in the upper and lower respiratory tracts, and induced systemic and nasal mucosal Th17 responses, high levels of PspA-specific serum immunoglobulin G (IgG), and nasal and bronchial IgA antibody responses. Moreover, there was no sign of PspA delivery by nanogel to either the olfactory bulbs or the central nervous system after intranasal administration. These results demonstrate the effectiveness and safety of the nanogel-based PspA nasal vaccine system as a universal mucosal vaccine against pneumococcal respiratory infection.

The use of polysaccharide-based injectable multivalent pneumococcal conjugate vaccines (PCV7, -10, and -13) has diminished the number of fatal infections due to pneumococci expressing the particular polysaccharides present in the vaccine (1–3). However, *Streptococcus pneumoniae* remains a problematic pathogen (4, 5) because of the large number of different capsular polysaccharides associated with virulent disease in humans. In particular, nonvaccine strains are emerging pathogens that result in morbidity and mortality due to pneumococcal diseases, including pneumonia and meningitis (6–8).

Clinical demand to overcome these problems has prompted the preclinical development of universal serotype-independent pneumococcal vaccines that are based on a surface protein common to all strains. Pneumococcal surface protein A (PspA), a pneumococcal virulence factor (9–13), is genetically variable (14) but highly cross-reactive (9, 10). PspA is commonly expressed by all capsular serotypes of *S. pneumoniae* (15) and is classified into 3 families (family 1, clades 1 and 2; family 2, clades 3 through 5; and family 3, clade 6) according to sequence similarities (14). Given that parenteral immunization with PspA induces cross-reactive neutralizing immune responses in mice (16–18) and humans (19), using PspA as a serotype-independent common antigen for the development of pneumococcal vaccines seems to be an ideal strategy.

Pneumococcal infection is generally preceded by colonization of the upper airway (20, 21). Nasal carriage of pneumococci is the primary source for spread of the infection among humans (22, 23). Therefore, an optimal vaccine strategy to prevent and control the spread of pneumococcal disease would induce protective immunity against both colonization and invasive disease. Several studies have confirmed the efficacy of PspA as a nasal vaccine antigen by coadministering PspA with a mucosal adjuvant such as cholera toxin (CT) or cholera toxin subunit B (CTB) to mice (24–26). The mice subsequently mount antigen-specific immune responses in not only the systemic compartment but also the respiratory mucosal compartment (24, 25, 27), where bacterial colonization occurs (20). PspA-specific secretory immunoglobulin A (sIgA) antibodies induced by intranasal immunization with PspA and an adjuvant (i.e., a plasmid expressing Flt3 ligand cDNA) provide protection against pneumococcal colonization (28). In addition, studies in mice have revealed that this protection is mediated by antigen-specific interleukin 17A (IL-17A)-secret-

Received 20 February 2013 Accepted 21 February 2013
Published ahead of print 4 March 2013
Editor: R. P. Morrison
Address correspondence to Hiroshi Kiyono, kiyono@ims.u-tokyo.ac.jp, or Yoshikazu Yuki, yukiy@ims.u-tokyo.ac.jp.
Supplemental material for this article may be found at http://dx.doi.org/10.1128/IAI.00240-13.

doi:10.1128/IAI.00240-13

ing $CD4^+$ T cells induced by intranasal immunization with pneumococcal whole-cell antigen (29, 30).

Therefore, the intranasal vaccination route is an improved route for preventing colonization of the nasal cavity by pneumococci. A leading obstacle to the practical use of nasal vaccine with a protein-based pneumococcal antigen is the need to coadminister a toxin-based mucosal adjuvant (e.g., CT) for effective induction of antigen-specific immune responses (31, 32). However, the use of such toxin-based adjuvants is undesirable in humans, as it carries the concern that the toxin may reach the central nervous system (CNS) or redirect the vaccine antigen into the CNS through the olfactory nerve in the nasal cavity (33, 34). To bypass these concerns, we recently developed a nasal vaccine delivery system based on a non-toxin-based mucosal antigen carrier, a cationic cholesteryl pullulan (cCHP) nanogel (35).

Here we show the efficacy of a nanogel-based nasal pneumococcal vaccine in which PspA is incorporated into a cCHP nanogel (cCHP-PspA). We also characterized the cCHP-PspA-induced PspA-specific Th17 and antibody responses against *S. pneumoniae*. Mice immunized with nasal cCHP-PspA were protected from lethal challenge with *S. pneumoniae* and had fewer pneumococci on their respiratory mucosae. These results suggest that a nontoxic nasal vaccine comprising nanogel-based PspA offers a practical and effective strategy against pneumococcal infection by preventing both nasal colonization and invasive diseases.

MATERIALS AND METHODS

Mice. Female BALB/c mice (aged 6 to 7 weeks) were purchased from SLC (Shizuoka, Japan). All of the mice were housed with *ad libitum* food and water on a standard 12-h–12-h light-dark cycle. All experiments were performed in accordance with the guidelines provided by the Animal Care and Use committees of the University of Tokyo and were approved by the Animal Committee of the Institute of Medical Science of the University of Tokyo.

Recombinant PspA. Recombinant PspA of *S. pneumoniae* Rx1, which belongs to PspA family 1, clade 2 (14), was prepared as described previously, with slight modifications (26). Briefly, a plasmid encoding PspA/Rx1 (pUAB055; amino acids 1 through 302) (GenBank accession no. M74122) was used to transform *Escherichia coli* BL21(DE3) cells. This construct contains amino acids 1 through 302 of the PspA protein from strain Rx1 plus a 6×His tag at the C terminus (26). The sonicated cell supernatant was loaded onto a DEAE-Sepharose column (BD Healthcare, Piscataway, NJ) and a nickel affinity column (Qiagen, Valencia, CA). This was followed by gel filtration on a Sephadex G-100 column (BD Healthcare).

Preparation of cCHP-recombinant PspA complex for intranasal vaccination. A cCHP nanogel (size, ~40 nm) generated from a cationic cholesteryl group-bearing pullulan was used for all experiments. The cCHP-PspA complex for each immunization was prepared by mixing 7.5 μg PspA with cCHP at a 3:1 molecular ratio (volume, 18 μl per mouse) and incubating the mixture for 1 h at 45°C. Before the complex was used in *in vivo* studies, the fluorescence resonance energy transfer (FRET) of fluorescein isothiocyanate (FITC)-PspA and a tetramethyl rhodamine isothiocyanate (TRITC)-cCHP nanogel was measured with a fluorescence spectrometer (model FP-6500; Jasco, Easton, MD) as described previously (37). FRET analyses confirmed that the cCHP nanogel appropriately formed nanoparticles after the incorporation of PspA (see Fig. S1 in the supplemental material). Dynamic light scattering analysis showed that the cCHP nanogel maintained the same nanoscale size (32.8 ± 0.2 nm) even after the incorporation of PspA. Lipopolysaccharide (LPS) contamination of purified PspA and cCHP (<10 endotoxin units/mg protein) was measured with a *Limulus* test (Wako, Osaka, Japan).

Immunization. Once weekly for 3 consecutive weeks, female BALB/c mice were immunized intranasally with cCHP-PspA, PspA plus CT (1 μg; List Biological Laboratory, Campbell, CA), PspA alone, or phosphate-buffered saline (PBS) only. Some experiments included an irrelevant antigen as a control; in these studies, mice were immunized intranasally with a complex of cCHP nanogel and a recombinant nontoxic receptor-binding fragment of *Clostridium botulinum* type A neurotoxin subunit antigen Hc (cCHP-BoHc/A) (35). Serum, nasal wash fluid (NW), and bronchoalveolar lavage fluid (BALF) samples were harvested 1 week after the last immunization. For NWs, 200 μl sterile PBS was flushed through the posterior choanae (38). BALF was harvested by instilling 1 ml of sterile PBS through a blunt needle placed in the trachea (38).

Bacterial strain. We used the kanamycin-resistant pneumococcal strain *S. pneumoniae* Xen10 (Caliper Life Sciences, MA), derived from the wild-type strain A66.1, which expresses PspA of family 1, clades 1 and 2 (39). *S. pneumoniae* Xen10 carries a stable copy of the modified *Photorhabdus luminescens lux* operon at a single integration site on the bacterial chromosome (40). The virulence of *S. pneumoniae* Xen10 is comparable to that of the parent strain (40, 41). For challenge studies, *S. pneumoniae* 3JYP3670, which expresses PspA of family 2, clade 4, was used (10). All of the *S. pneumoniae* strains were grown in brain heart infusion (BHI) broth at 37°C in 5% CO_2.

Pneumococcal infection model. To evaluate the efficacy of intranasal vaccination with cCHP-PspA, mice were challenged 1 week after the last immunization. The cell densities of exponentially growing *S. pneumoniae* Xen10 cultured at 37°C in BHI broth were estimated from the optical density at 600 nm (OD_{600}); cells were pelleted and then diluted with PBS. Lethal (2×10^5 CFU) and sublethal (2×10^4 CFU) challenge doses diluted in 50 μl sterile PBS were administered intranasally to isoflurane-anesthetized mice. Mice were restrained vertically for 5 min to ensure inhalation of the organisms into the trachea. In addition, mice were inoculated intranasally with a lethal challenge dose (5×10^4 CFU) of strain 3JYP3670 in the same way as that for strain Xen10. Nasal passages and lung tissues were homogenized in 500 μl sterile PBS for 1 min, and the numbers of bacterial colonies were determined by plating samples on LB agar plates containing kanamycin (200 μl/ml).

***In vivo* imaging of immunized and challenged mice.** Bioluminescence of bacteria was monitored for 1 min 24, 48, and 72 h after lethal challenge by using an Ivis charge-coupled device (CCD) camera (Xenogen, Alameda, CA). Total photon emission from the entire thorax of each mouse was quantified by using the LivingImage software package (Xenogen). The results are provided as numbers of photons/s/cm^2/sr.

Antibody titer and subclass analysis. Antibody titers were determined by using enzyme-linked immunosorbent assay (ELISA) as described previously, with slight modifications (25). In brief, samples (2-fold serial dilutions) were loaded into individual wells, and the plate was coated with 1 μg/ml recombinant PspA and incubated. Goat anti-mouse IgA, IgG, IgG1, IgG2a, IgG2b, IgG3, and IgM (dilution factor, 1:4,000) conjugated with horseradish peroxidase were used as secondary antibodies. Reactions were visualized by using the TMB microwell peroxidase substrate system (XPL, Gaithersburg, MD). The endpoint titer is expressed as the reciprocal $\log_2$ of the last dilution that gave an OD_{450} that was 0.1 unit greater than that of the negative control.

PspA-specific $CD4^+$ T cell responses. By using anti-CD4 microbeads (Miltenyi Biotec, Sunnyvale, CA) according to the manufacturer's instructions, $CD4^+$ T cells were isolated from the spleens and cervical lymph nodes (CLNs) of mice intranasally immunized with cCHP-PspA, PspA alone, or PBS only. The purified $CD4^+$ T cells were resuspended at 1×10^6 cells/ml in RPMI 1640 (Cellgro, Mediatech, Washington, DC) supplemented with 10 mM HEPES, 50 μM 2-mercaptoethanol, 100 U/ml penicillin, 100 μl/ml streptomycin, and 10% fetal calf serum and then cocultured with irradiated (2,000 rad) splenic antigen-presenting cells (2×10^6 cells/ml) from naïve BALB/c mice for 5 days at 37°C in 5% CO_2 in the presence of 1 μg/ml PspA. Cytokine levels in $CD4^+$ T cell culture supernatants were determined by using cytokine-specific DuoSet ELISA kits

(R&D Systems, Minneapolis, MN) according to the manufacturer's instructions.

Radioisotope counting assay. To trace the distribution of PspA after intranasal immunization, PspA was labeled with indium chloride (Nihon Medi-Physics, Tokyo, Japan) anhydride (Dojindo, Kumamoto, Japan) via N-terminal and ε-Lys amino groups, using diethylenetriaminepentaacetic acid as described previously (42). ^{111}In-labeled PspA was administered alone or as a complex with cCHP nanogel. The radioisotope counts in the nasal passage, olfactory bulbs, and brain 10 min and 1, 6, 12, 24, and 48 h after instillation were estimated with a γ-counter (Wizard model 1480; PerkinElmer, Waltham, MA). The results are provided as standardized uptake values (SUVs), calculated as radioisotope counts (cpm) per gram of tissue divided by the ratio of the injected dose (1×10^6 cpm) to body weight (in grams).

Flow cytometric analysis. Mice were immunized intranasally with FITC-PspA in cCHP nanogel, FITC-PspA alone, or PBS only; 6 h later, mononuclear cells were prepared from the nasal passages of each group by mechanical dissociation through 70-μm nylon mesh, as described previously (38, 43). Isolated cells were stained with phycoerythrin (PE)-Cy7-conjugated anti-CD11c (BD Bioscience) and analyzed by flow cytometry. The percentage of PspA$^+$ cells in the CD11c$^+$ fractions was calculated for each experimental group.

Data analysis. Data are expressed as means ± standard deviations (SD). Statistical analysis for most comparisons among groups was performed with Tukey's *t* test; differences were considered statistically significant when the *P* value was <0.05. For survival data, the Fisher exact test was used to compare the numbers of alive versus dead mice in the cCHP-PspA, PspA-CT, and PBS-only groups with those in the PspA-only group.

RESULTS

Intranasal vaccination with cCHP-PspA induces protective immunity against lethal challenge with *S. pneumoniae*. To evaluate whether intranasal cCHP-PspA vaccination induces protective immunity against pneumococcal challenge, we vaccinated mice with cCHP-PspA, PspA-CT, PspA alone, or PBS only. One week after the last immunization, we lethally challenged vaccinated mice with the virulent strain *S. pneumoniae* Xen10 (2×10^5 CFU), which is *S. pneumoniae* A66.1 rendered bioluminescent by the integration of a modified *lux* operon into its chromosome (40). The PspA expression level of strain Xen10 was confirmed to be comparable to that of the parent strain (see Fig. S2 in the supplemental material). We then evaluated survival rates after lethal challenge over a 2-week period. The survival rate of the cCHP-PspA-vaccinated group was 100%, as was that for PspA-CT-vaccinated mice (Fig. 1). In contrast, most of the mice intranasally immunized with PspA alone (survival rate, 0%) or with PBS (20% survival) died within 8 days of challenge with *S. pneumoniae* Xen10 (Fig. 1). The survival rates of the groups immunized with cCHP-PspA or PspA-CT were higher and were statistically significant compared to that of the group immunized with PspA alone ($P < 0.01$). The results from the PspA-only and PBS-only groups did not differ ($P > 0.05$). In addition, immunization with the irrelevant antigen BoHc/A incorporated into cCHP (cCHP-BoHc/A) (35) did not protect mice from challenge with *S. pneumoniae* Xen10 (see Fig. S3). Because PspA family 2 (clades 3 through 5) and family 1 (clades 1 and 2) constitute 94 to 99% of clinical isolates of pneumococci (14, 44–49), we also challenged mice with the strain 3JYP3670, which expresses PspA belonging to clade 4 of family 2 (10). Unlike mice inoculated with cCHP-BoHc/A, PspA alone, or PBS only, mice nasally immunized with cCHP-PspA were protected from lethal challenge with 3JYP3670

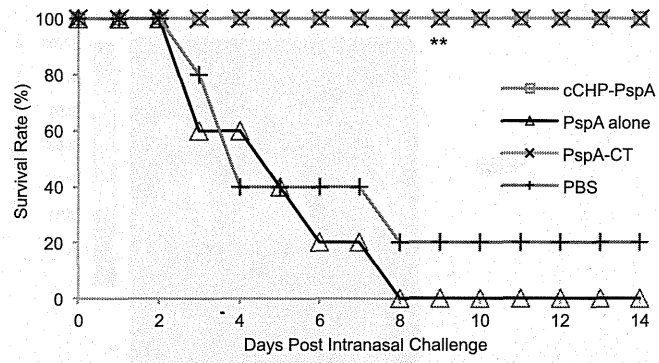

FIG 1 Intranasal vaccination with cCHP-PspA induced protective immunity against pneumococci. One week after the final immunization, mice were challenged with *S. pneumoniae* Xen10 (2×10^5 CFU/mouse), and survival was monitored. Data are representative of three independent experiments, and each group consisted of 5 mice. *P* values were calculated by using the Fisher exact test to compare the numbers of alive versus dead mice in each group with the result obtained for the PspA-only group. **, $P < 0.01$ compared with the group immunized with PspA alone. Abbreviations: cCHP, cationic cholesteryl group-bearing pullulan; CT, cholera toxin; PspA, pneumococcal surface protein A.

(PspA of clade 4) (10), as was the case with Xen10 expressing PspA of clades 1 and 2 (see Fig. S4).

Intranasal vaccination with cCHP-PspA enhances bacterial clearance from BALF and the lung. To assess whether intranasal immunization with cCHP-PspA prevented pulmonary infection with pneumococci, we performed *in vivo* bioluminescence imaging of *S. pneumoniae* Xen10 after lethal challenge (2×10^5 CFU) of mice intranasally vaccinated with cCHP-PspA, PspA alone, or PBS. The lungs of mice immunized with PspA alone or with PBS only (control group) showed high-intensity photon signals in a pattern consistent with that of full-blown lung infection (Fig. 2A). In contrast, the lungs of mice immunized with cCHP-PspA lacked bioluminescence, indicating the absence of pulmonary infection. Forty-eight and 72 h after infection, photon counts of the cCHP-PspA-vaccinated group were significantly lower than those of the other two groups (Fig. 2B).

To investigate whether intranasal immunization with cCHP-PspA hastened bacterial clearance from the lung, we counted the bacteria in the BALF and lung tissues of mice intranasally vaccinated with cCHP-PspA, PspA alone, or PBS and sublethally challenged with *S. pneumoniae* Xen10 (2×10^4 CFU). Three hours after challenge, bacterial numbers in BALF (Fig. 2C) and lung tissue (Fig. 2D) did not differ among the three vaccination groups. However, 24 h after challenge, the bacterial counts in the BALF and lung homogenates from the cCHP-PspA-vaccinated groups were significantly lower (about 100-fold) than those for the mice immunized with PspA alone or PBS only (Fig. 2C and D).

Intranasal vaccination with cCHP-PspA reduces bacterial colonization in the nasal cavity. We next examined whether intranasal cCHP-PspA immunization affected nasal carriage of pneumococci in mice challenged with *S. pneumoniae* Xen10. Three days after challenge, bacterial numbers in NWs (Fig. 3A) and nasal passages (Fig. 3B) of mice immunized with the cCHP-PspA nasal vaccine were decreased significantly (approximately 100-fold) compared to those for the two control groups.

Intranasal vaccination with cCHP-PspA induces strong Th17 and Th2 responses. We then examined the type of immune

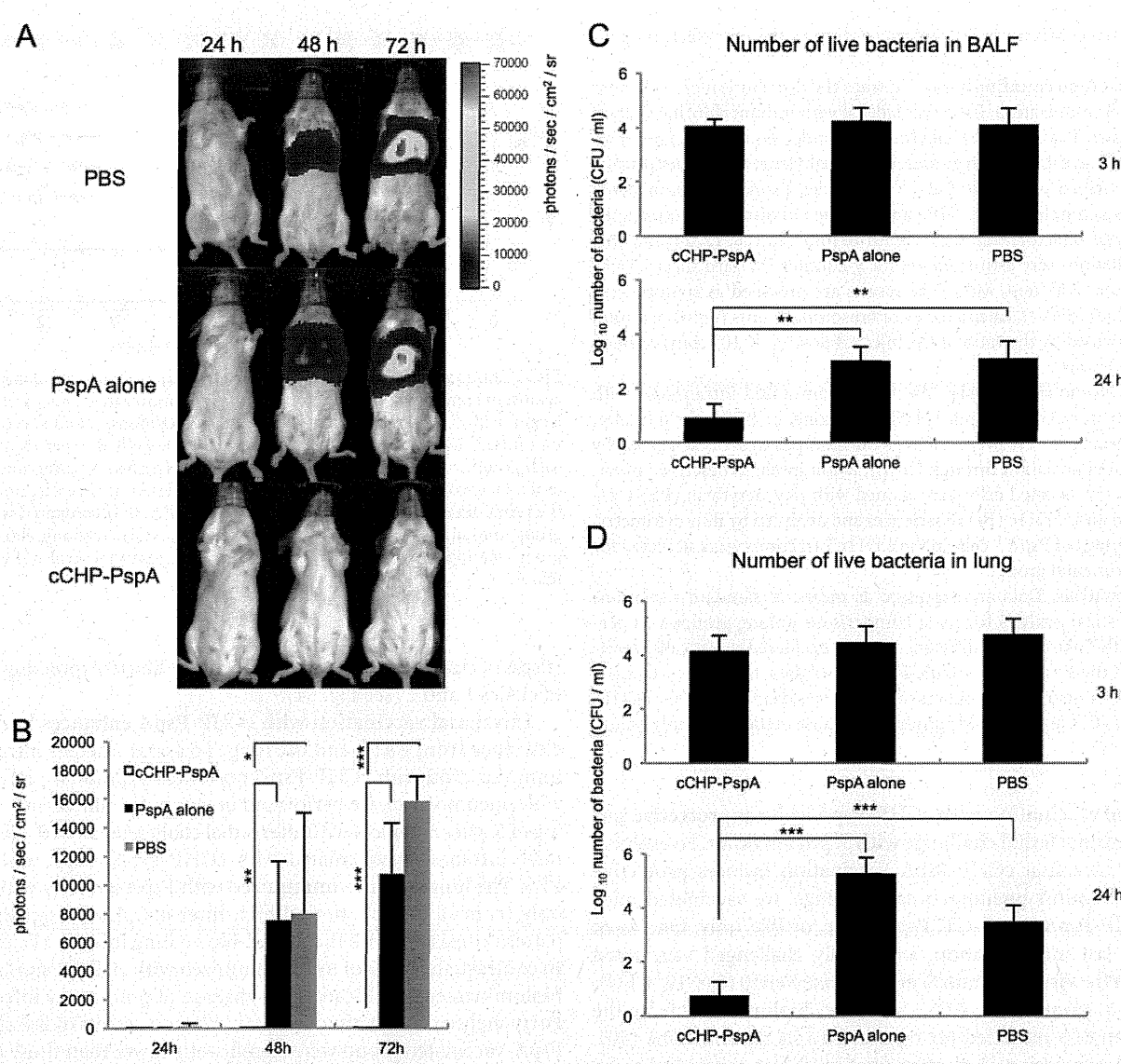

FIG 2 *In vivo* imaging revealed no sign of pneumococcal infection in the lungs of mice immunized intranasally with cCHP-PspA; these mice also showed enhanced bacterial clearance from the BALF and lung. Images (A) and average photon counts (B) show bioluminescence due to *S. pneumoniae* Xen10 in each group of mice infected intranasally with *S. pneumoniae* Xen10 (2×10^5 CFU/mouse) and imaged 24, 48, and 72 h after infection. (C and D) One week after the final immunization, mice were challenged with a sublethal dose (2×10^4 CFU/mouse) of *S. pneumoniae* Xen10. BALF and lung tissues were collected, and the numbers of *S. pneumoniae* Xen10 organisms 3 and 24 h after challenge were determined. Data are representative of three independent experiments, and each group consisted of 5 mice. *, $P < 0.05$; **, $P < 0.01$; ***, $P < 0.001$. Abbreviations: BALF, bronchoalveolar lavage fluid; cCHP, cationic cholesteryl-group-bearing pullulan; PspA, pneumococcal surface protein A.

responses elicited by intranasal cCHP-PspA vaccination. Compared with PspA alone or PBS, cCHP-PspA induced higher levels of IL-17 in $CD4^+$ T cells from the spleen, CLNs, and nasal passages (Fig. 4A). The cCHP-PspA-vaccinated group produced high levels of IL-4 and IL-13, the hallmark cytokines of a Th2-type immune response, but only scant amounts of gamma interferon (Fig. 4B to D). These results show the potential of a cCHP-PspA nasal vaccine as an advanced pneumococcal vaccine that can induce a Th17 response together with a Th2-type immune response.

Intranasal vaccination with cCHP-PspA induces high levels of systemic antibodies. To address whether intranasal administration of cCHP-PspA induced PspA-specific antibody responses, we examined the serum titers of PspA-specific antibodies. PspA-specific IgG responses in the systemic compartment were significantly higher in mice immunized with intranasal cCHP-PspA than in those given PspA only (Fig. 5A). Unlike the predominant IgG response, IgM and IgA titers in the serum samples were very low (Fig. 5A).

Intranasal immunization with cCHP-PspA induced primarily IgG1 antibodies, followed by IgG2b antibodies (Fig. 5B). This pattern indicated skewing toward a Th2-type response and was consistent with the cytokine profiles of the culture supernatants from antigen-stimulated $CD4^+$ T cells prepared from the same mice (Fig. 4B and C).

Intranasal vaccination with cCHP-PspA induces high levels of mucosal antigen-specific sIgA antibodies. We next examined whether vaccinated mice also produced mucosal antigen-specific Ig responses. Intranasal vaccination with cCHP-PspA induced

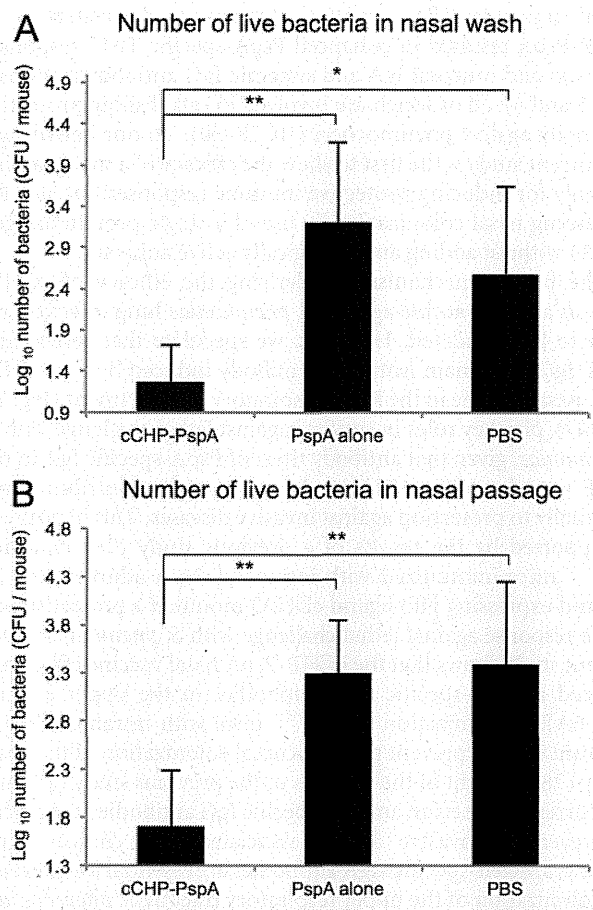

FIG 3 Intranasal vaccination with cCHP-PspA reduced bacterial colonization of the nasal cavity. One week after the final immunization, mice were challenged with a sublethal dose (2×10^4 CFU/mouse) of *Streptococcus pneumoniae* Xen10. Nasal washes and tissues were collected, and the numbers of *S. pneumoniae* Xen10 3 days after infection were determined. Data are representative of three independent experiments, and each group consisted of 5 mice. *, $P < 0.05$; **, $P < 0.01$. Abbreviations: cCHP, cationic cholesteryl group-bearing pullulan; PspA, pneumococcal surface protein A.

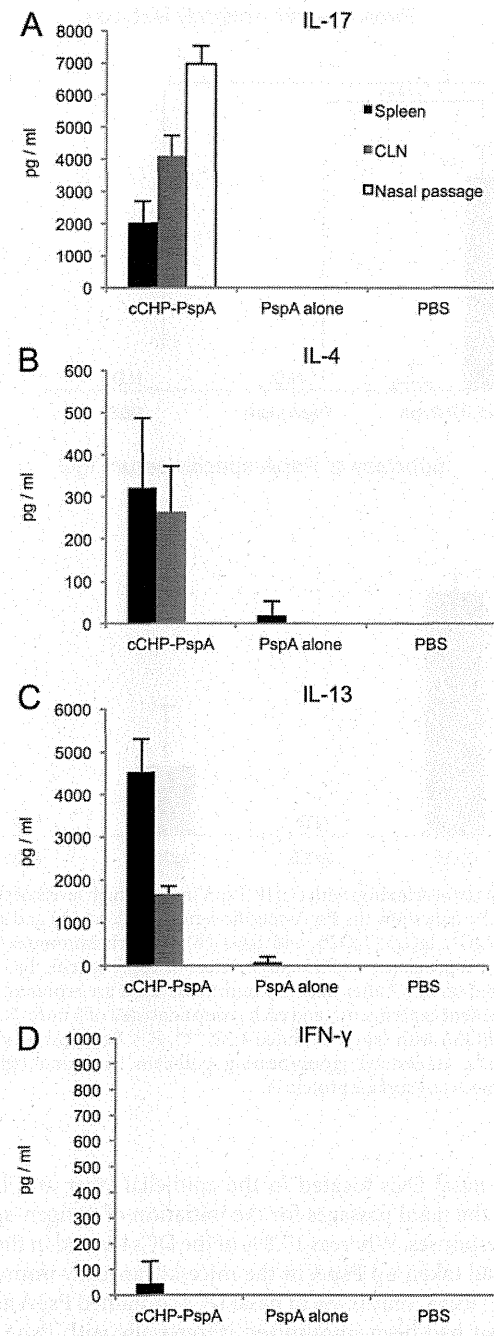

FIG 4 $CD4^+$ T cells from cCHP-PspA-immunized mice produce Th17- and Th2-type immune responses. Cytokines produced by $CD4^+$ T cells isolated from the spleens, cervical lymph nodes, and nasal passages of mice immunized with cCHP-PspA, PspA alone, or PBS only were analyzed. Data are representative of five independent experiments, and each group consisted of 5 mice. Abbreviations: cCHP, cationic cholesteryl-group-bearing pullulan; CLN, cervical lymph node; IFN-γ, gamma interferon; IL, interleukin; PspA, pneumococcal surface protein A.

PspA-specific mucosal IgA antibodies in the nasal secretions (Fig. 6A). In addition, BALF samples from mice intranasally vaccinated with cCHP-PspA contained PspA-specific IgA antibodies (Fig. 6B), and PspA-specific IgG antibodies were detected at high titers in both the NWs and BALF of mice intranasally immunized with cCHP-PspA (Fig. 6C and D). The nasal and BALF antigen-specific IgGs induced by intranasal immunization with cCHP-PspA were primarily of the IgG1 and IgG2b subclasses (Fig. 6E and F), similar to the Ig responses in the systemic compartment (Fig. 5B). Taken together, these results further support the benefit of cCHP-based nanogel as an effective nasal vaccine delivery vehicle for the induction of PspA-specific systemic and mucosal antibody responses against *S. pneumoniae*.

cCHP delivers PspA to dendritic cells (DCs) without CNS accumulation of PspA. The potential for antigen deposition and accumulation in the CNS through the olfactory fossa is one of the great concerns surrounding the use of nasal vaccines (33, 34, 50). To address this important concern, we instilled ^{111}In-labeled PspA alone or in complex with cCHP into the nasal cavities of mice. Beginning 6 h after administration, the nasal passages of mice treated with ^{111}In-labeled cCHP-PspA had higher SUVs than did those of mice treated with ^{111}In-labeled PspA alone, but there was no accumulation of ^{111}In-labeled PspA in the olfactory bulbs or brain throughout the 48-h observation period (Fig. 7A).

The cCHP vaccine delivery system enabled prolonged antigen exposure at the nasal epithelium, allowing continuous antigen

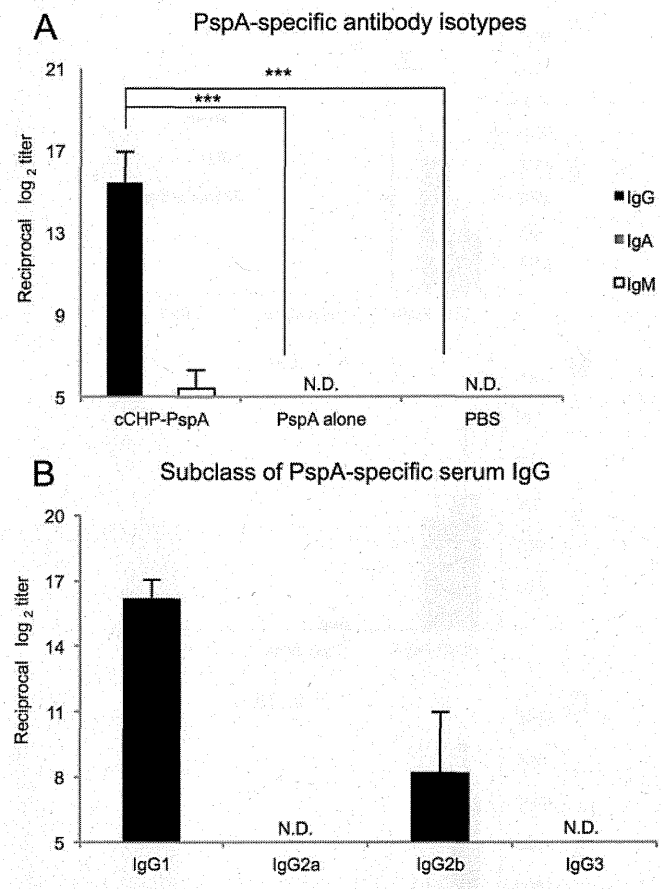

FIG 5 Intranasal vaccination with cCHP-PspA induced high levels of systemic antibodies. The data show the PspA-specific serum IgG level (A) and subclass analysis for IgG1, IgG2a, IgG2b, and IgG3 (B) for each immunized group (cCHP-PspA, PspA alone, or PBS only). Titers of PspA-specific IgG in sera were measured on day 7 after final immunization. Data are representative of three independent experiments, and each group consisted of 5 mice. N.D., not detected by ELISA with samples diluted 1:32. ***, $P < 0.001$. Abbreviations: cCHP, cationic cholesteryl group-bearing pullulan; Ig, immunoglobulin; PspA, pneumococcal surface protein A.

uptake by nasal DCs located in the epithelial layer and lamina propria of the nasal passages for the initiation of antigen-specific immune responses. Whereas 17.8% of the DCs located in the nasal passages had taken up PspA in the mice intranasally immunized with cCHP-PspA, only 0.7% of nasal DCs contained PspA antigen in mice that had been immunized intranasally with PspA alone (Fig. 7B). These results further support the concept that the cCHP-PspA vaccine formulation is an attractive inhalant delivery vehicle that effectively delivers and sustains antigen at the nasal epithelium for continuous antigen uptake by DCs without antigen deposition in the CNS.

DISCUSSION

We showed that cCHP-PspA-vaccinated mice survived a lethal challenge with *S. pneumoniae* (Fig. 1; see Fig. S4 in the supplemental material), whereas mice vaccinated with cCHP complexed with an irrelevant antigen (BoHc/A) did not (see Fig. S3 and S4). Importantly, compared with those of mice inoculated with control constructs, the respiratory tracts of mice immunized with intranasal cCHP-PspA had less colonization and invasion by pneumococcal organisms (Fig. 2 and 3). Intranasal administration of cCHP-PspA resulted in enhanced PspA-specific Th17 responses (Fig. 4A) and mucosal IgA and systemic IgG antibody responses (Fig. 5 and 6), all of which are involved in establishing protective immunity against pneumococci (10, 28–30). To our knowledge, the current study is the first to show the efficacy of a nasal vaccine not only for inducing protective immune responses but also for preventing nasal colonization by use of a single protein antigen (PspA) without adding any biologically active adjuvant.

The precise mechanisms underlying the efficacy of cCHP-PspA as a nasal vaccine against *S. pneumoniae* lung infection remain to be elucidated. However, we speculate that serum and BALF IgGs, the main isotype of antibody induced by the cCHP-PspA nasal vaccine in the lower respiratory compartment (Fig. 5A and 6D), play key roles in survival against lethal challenge with *S. pneumoniae*, given that antibody titers of PspA-specific IgA in the BALF were low (Fig. 6B) and therefore might contribute only minimally to protection against invasive diseases. This hypothesis is supported by the results of a previous study (28) in which $IgA^{-/-}$ mice immunized with intranasal PspA-adjuvant (i.e., a plasmid expressing Flt3 ligand cDNA) mounted a protective immune response against lethal challenge with *S. pneumoniae*. Our current study shows that the cCHP-PspA nasal vaccine effectively induced antigen-specific sIgA antibodies in the upper airways (Fig. 6A). Immunization of $IgA^{-/-}$ mice with intranasal PspA-adjuvant did not prevent pneumococcal colonization of the nasal cavity (28). In light of the findings of the previous study (28) and our current one, serum antigen-specific IgG antibodies are crucial to preventing invasive disease associated with clinical signs, whereas antigen-specific sIgA antibodies are essential for preventing colonization of the upper respiratory tract by *S. pneumoniae*.

In addition to the essential role of sIgA in protection from nasopharyngeal colonization by pneumococci, IL-17A-producing $CD4^+$ T cells play an important role in preventing pneumococcal nasal colonization in mice immunized with intranasal pneumococcal whole-cell antigen (29, 30). Recent studies have found that IL-17 promotes multiple aspects of humoral immunity by enhancing B cell proliferation and isotype switching (51), B cell recruitment to the respiratory mucosa, and expression of the polymeric immunoglobulin receptor on the airway epithelium (52). In the current study, we found that intranasal immunization with cCHP-PspA generated Th17 cells in the nasal passages, draining lymph nodes, and systemic compartment (Fig. 4A). Therefore, our findings suggest that intranasal immunization with cCHP-PspA induces both humoral and cellular immune responses, which are required for protective immunity against pneumococcal colonization and invasive disease. In addition to their essential role in antipneumococcal immunity (29, 30), Th17 responses are a hallmark of autoimmunity (53). Therefore, future studies should carefully examine whether the Th17 responses induced by intranasal immunization with cCHP-PspA are associated with any adverse effects.

As one might expect, the protective immunity induced by nasal cCHP-PspA was not observed when an irrelevant antigen, BoHc/A, was incorporated into cCHP (cCHP-BoHc/A) (35) and used as a nasal vaccine (see Fig. S3 and S4 in the supplemental material). Moreover, mice immunized intranasally with cCHP-PspA (PspA of clades 1 and 2) were protected against challenge with pneumococcal strain 3JYP3670, which expresses PspA of clade 4 (10), whereas mice immunized with cCHP-BoHc/A, PspA